

Fluid Mechanics of Aquatic Locomotion at Large Reynolds Numbers

*R.N. Govardhan and J.H. Arakeri**

Abstract | There exist a huge range of fish species besides other aquatic organisms like squids and salps that locomote in water at large Reynolds numbers, a regime of flow where inertial forces dominate viscous forces. In the present review, we discuss the fluid mechanics governing the locomotion of such organisms. Most fishes propel themselves by periodic undulatory motions of the body and tail, and the typical classification of their swimming modes is based on the fraction of their body that undergoes such undulatory motions. In the anguilliform mode, or the eel type, the entire body undergoes undulatory motions in the form of a travelling wave that goes from head to tail, while in the other extreme case, the thunniform mode, only the rear tail (caudal fin) undergoes lateral oscillations. The thunniform mode of swimming is essentially based on the lift force generated by the airfoil like cross-section of the fish tail as it moves laterally through the water, while the anguilliform mode may be understood using the “reactive theory” of Lighthill. In pulsed jet propulsion, adopted by squids and salps, there are two components to the thrust; the first due to the familiar ejection of momentum and the other due to an over-pressure at the exit plane caused by the unsteadiness of the jet. The flow immediately downstream of the body in all three modes consists of vortex rings; the differentiating point being the vastly different orientations of the vortex rings. However, since all the bodies are self-propelling, the thrust force must be equal to the drag force (at steady speed), implying no net force on the body, and hence the wake or flow downstream must be momentumless. For such bodies, where there is no net force, it is difficult to directly define a propulsion efficiency, although it is possible to use some other very different measures like “cost of transportation” to broadly judge performance.

1. Introduction

The Earth's oceans, rivers and lakes contain a very large number of fish species about 28,000 (Nelson, 2006), which have adapted to the varied habitats and evolved into a wide range of interesting morphology and fin structures, as may be seen for example in the book by Nelson (2006). These fishes and other aquatic creatures, such as squids,

salps and scallops, have also evolved and most likely optimized (for their requirements) varied mechanisms for locomotion in water. Most of the fishes locomote by undulatory motions of their body and tail, while some other aquatic creatures get their propulsive thrust from pulsed jets. In this paper, we present an overview of the fluid mechanics underlying the broad strategies adopted by these

Department of
Mechanical Engineering
Indian Institute of
Science Bangalore
560012, India
*jaywant@mecheng.iisc.ernet

organisms for locomotion. As stated in the title of the paper, we consider only locomotion at large Reynolds numbers ($Re = U_b L/\nu \gg 1$), where U_b is the typical swimming speed, L is the characteristic size of the organism and ν is the kinematic viscosity of water ($\nu = 10^{-6} \text{ m}^2/\text{s}$). Broadly this covers all marine life that is larger than about a centimeter and travelling at speeds greater than a centimeter per second ($Re > 100$), and includes a whole range of aquatic organisms ranging from small fishes ($Re \approx 10^3$) to the large blue whale ($Re \approx 10^8$) and also including a range of other aquatic creatures as given in table 1. Large Reynolds numbers ($Re > 100$) would imply in simple terms that inertial forces on the body are large compared to viscous forces on the body, in contrast to micro-organisms with $Re \ll 1$, where viscous forces dominate and whose locomotion is quite different as reviewed in Subramaniam and Nott (2011). There exists a large amount of literature on the subject of aquatic locomotion, including several review papers on different aspects of fish swimming (Triantafyllou, Triantafyllou & Yue, 2000; Fish & Lauder, 2006; Wu, 2011); and some books (Lighthill, 1975; Videler, 2003), and hence the focus of this paper is only to give an overview of the field with references to some important studies.

Some broad features differentiate aquatic locomotion from both terrestrial and aerial

locomotion of large organisms. Aquatic organisms have to be able to move in the bulk of the fluid (water) generally far away from solid ground, and in a medium where their own body densities are nearly matched with that of the surrounding fluid; the first point differentiates them from terrestrial animals and the second point from flying birds and insects. Nearly all aquatic organisms are close to neutrally buoyant in water, which implies that they need only to provide thrust for locomotion from their undulatory motions and do not need to generate a vertical lift force to balance gravity as in the case of birds and insects; the fluid mechanics of flight is discussed in an accompanying article. There are a few fishes, such as some sharks, where buoyancy does not balance weight, and they have evolved mechanisms to also generate a vertical lift force, although it should be noted that the percentage difference in densities would still be quite small compared to organisms flying in air.

The swimming of fishes has attracted interest from the times of Aristotle (Lindsey, 1978) to the present. Fishes in general locomote by the undulatory motions of their body and tail. The detailed motions of such swimming fishes have been recorded starting from Marey's (1895) use of cinematography, followed by the extensive work of Breder (1926) and Gray (1933 onwards), with the latter two bringing in mechanical analysis to

Table 1: Swimming kinematics and Reynolds numbers for a range of aquatic organisms. For each species, the body length (L), swimming speed (U), the normalized lateral tail (tip) amplitude (A/L), Reynolds number (Re), the body lengths/s (L/s), the stride or body lengths/beat and the wave speed (V) for fishes and jet speed (U_j) for squid is given. Data source: ¹Videler, (1993) (compilation); ²Tytell & Lauder (2004); ³Bartol et al. (2001); ⁴Anderson & Grosenbaugh (2005); ⁵Madin (1990).

Species	L (m)	U (m/s)	A/L	Re	L/s	L/beat	Wave speed (or) Jet speed
Blue Whale ¹	30.00	10.00		$3.0E + 08$	0.33		
Tuna ¹	3.00	10.00		$3.0E + 07$	3.33		
Atlantic Salmon ¹ (<i>Salmo Salar</i>)	0.67	2.37	0.05	$1.6E + 06$	3.56	0.67	$V = 1.35 U$
Atlantic Mackarel ¹ (<i>Scomber scombrus</i>)	0.30	1.35	0.10	$4.1E + 05$	4.50	0.80	$V = 1.43 U$
Rainbow trout ¹ (<i>Oncorhynchus mykiss</i>)	0.06	0.36	0.11	$2.0E + 04$	6.45	0.65	$V = 1.49 U$
	0.20	0.50	0.08	$1.0E + 05$	2.50	0.63	$V = 1.43 U$
American eel ² (<i>Anguilla rostrata</i>)	0.21	0.29	0.07	$6.0E + 04$	1.37	0.45	$V = 1.37 U$
Shallow water squid ³ (<i>Lolliguncula brevis</i>)	0.08	0.22		$1.8E + 04$	2.78	1.39	$U_j = 3.96 U$
Long-finned squid ⁴ (<i>Loligo pealei</i>)	0.27	0.59		$1.6E + 05$	2.19	1.68	$U_j = 1.15 U$
Salp ⁵ (<i>Cyclosalpa polae</i>)	0.06	0.03		$1.8E + 03$	0.60	0.86	

the swimming of fishes. It was Breder (1926) who first classified the different types of fish swimming modes, which is illustrated in figure 1 that is adapted from Lindsey (1978). The classification is essentially based on the fraction of the full body that undergoes undulatory motion. In the anguilliform mode (figure 1a), which is the eel type, almost the entire body undergoes undulatory motions, while in the thunniform mode, adopted by tuna and sharks, only the tail fin (caudal fin) undergoes oscillatory lateral motions. The carangiform and sub-carangiform modes fall in-between these modes as illustrated in the figure, with progressively smaller fractions of the body participating in the undulatory motions of the body. More recently, Lauder & Tytell (2006) have raised questions over this type of classification and suggest that the main differences between anguilliform and thunniform modes may not be related to the top view differences in motion shown in figure 1, but to the 3D structure of their bodies.

The undulatory motions of the fish result in lateral flapping motions of the tail that have associated with it a tail flapping frequency. This flapping frequency is typically non-dimensionalized by the lateral total excursion of the tail (A) and fish swimming speed (U) to form a non-dimensional Strouhal number, $St = fA/U$, which is important in determining the unsteady flow around the fish body. For example, laboratory

experiments on oscillating foils, an idealization of a fish tail cross-section, show that the thrust forces generated can vary substantially as the Strouhal number is varied. Measurements on live swimming fishes show that the Strouhal number for a large range of species lies in the range of 0.2 to 0.35 (Triantafyllou et al., 1993; Triantafyllou & Triantafyllou, 1995). Triantafyllou et al. (1993) suggest that this range of Strouhal number is optimal in terms of efficient thrust generation using direct measurements of efficiency of an oscillating foil (an idealized fish tail) at various Strouhal numbers and using wake instability analysis.

In many papers on actual fish locomotion, the forward motions of the fish are given in terms of either the body lengths moved per second (L/s) or as a "stride", which is the body lengths moved in one period of body/tail oscillation. These quantities for a range of aquatic creatures are also given in table 1, indicating that for almost all organisms the stride is of the order of unity. The table also lists the tail flapping amplitude normalized by the body length (A/L); A/L for most creatures is about 0.1.

Fishes have several fins that are used for propulsion and maneuvering. Figure 2 shows a picture taken in a small aquarium tank of a silver shark (*Balantiocheilus melanopterus*) and the nomenclature for the common fins. These include the caudal fin (tail), which is typically used for propulsion, the dorsal fin on top and

Wake: Wake refers to the disturbed flow downstream of a body. Typically, wake is a region in which there is lateral variation of the streamwise component of velocity downstream of a body.

Figure 1: Different fish swimming modes going from nearly whole body undulatory motion in (a) to predominantly caudal tail oscillatory motion in (d). (a) Anguilliform (e.g. eel), (b) Subcarangiform (e.g. trout), (c) Carangiform (e.g. bluefish), and (d) Thunniform (e.g. sharks). Figure is adapted from Lindsey (1978).

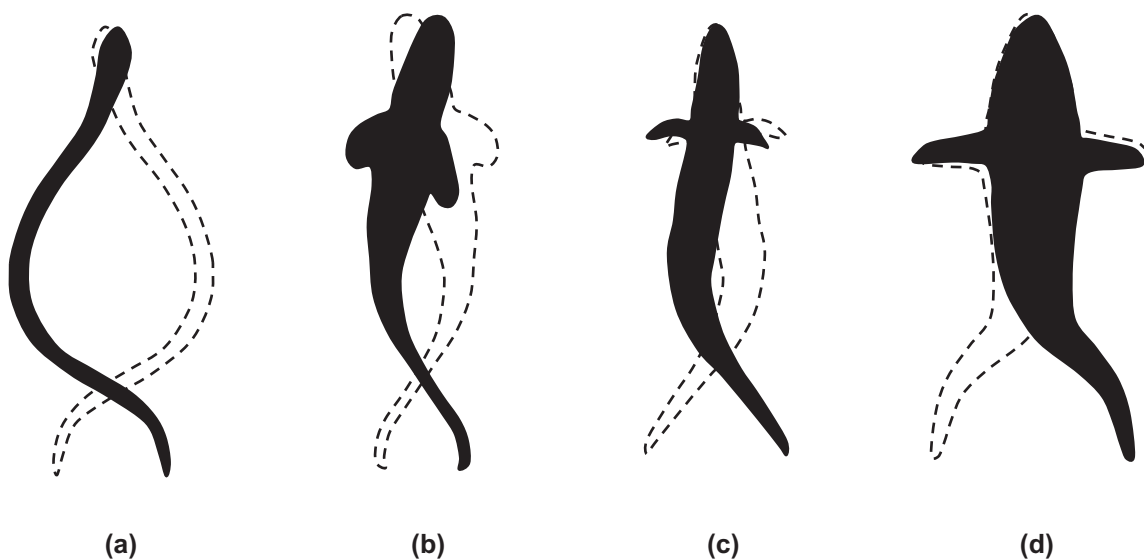
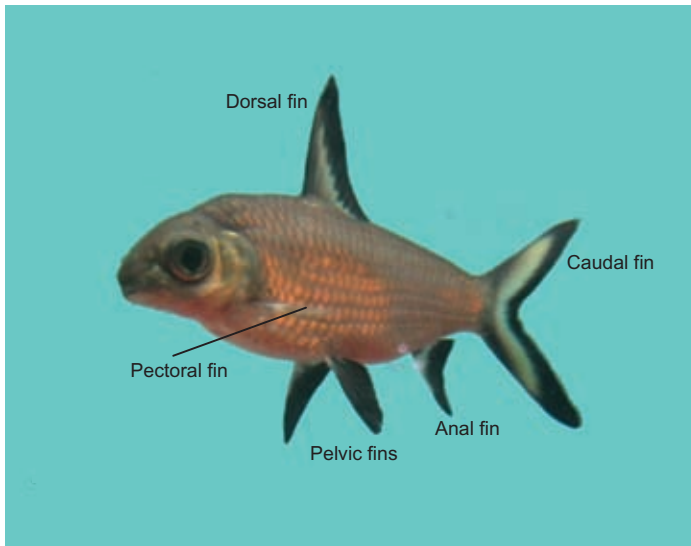


Figure 2: Photograph showing the different fins on a typical fish. The picture is of a Silver Shark (*Balantiocheilus melanopterus*). In this case, the dorsal, caudal, pelvic and anal fins have a dark prominent shading, while it is absent in the pectoral fins close to the head.



the anal fin at the bottom, all of which are in the central-plane of the fish. The pectoral and pelvic fins are in pairs and are placed symmetrically off the central-plane, and are usually used for control and maneuvering of the fish. Some fishes, such as shiner perch (*Cymatogaster aggregate*) and the rays (*Raja undulate*), use their pectoral fins for swimming. For a more complete view of the different fins on a fish, the reader is referred to the book by Nelson (2006). Whereas most fishes propel themselves by undulatory motions of their body and tail, other aquatic organisms, like squids, propel themselves using thrust from pulsed water jets. Shown in figure 3 is a schematic of a squid that draws in water from the surroundings into a cavity in the “mantle” and then shoots out a high-speed jet from the “funnel” to propel itself forward. This kind of propulsion clearly requires very different kind of adaptations and morphological features.

Any introduction on fish swimming is not complete without the statement of “Gray’s paradox” emanating from the work of Gray (1936). Simply stated Gray estimated that the power required for a dolphin to swim while overcoming its drag was about 7 times larger than the estimated power available based on its muscle mass. This has typically been interpreted as the ability of the fish to considerably reduce the drag on its body compared to the drag on a similar towed body (as was used in Gray’s estimate).

This sparked off enormous interest, as it held the possibility of considerably reducing the drag on man made aquatic vehicles, and is often quoted as one of the main driving reasons for studies on fish swimming. Although it is likely that there were issues with the estimates (and observations) done by Gray, as quoted by others over the years, it is likely that dolphins and other fishes have optimized their swimming motions to a degree that is better than our understanding of it.

In this article, we will be discussing mainly three of the known numerous modes of thrust generation, anguilliform mode, thunniform mode and pulsed jet propulsion. These three are not only the most commonly found, but also cover the main principles of thrust generation found in the other modes as well. Often, more than one of these basic modes may be present in one aquatic organism. We will be concerned with only constant velocity motion in this article, as motions involving accelerations, decelerations and turning, though interesting, haven’t been studied much, and are even less understood. We shall start by briefly discussing the force balance on self-propelling bodies, before proceeding on to the three modes of thrust generation. This will be followed by a discussion of momentum and energy in the wake, and then the wake structure. We end with some discussion and conclusions about the three modes and an overview of some of the important features of aquatic locomotion.

2. Force Balance on Self Propelling Bodies Moving with Constant Velocity

From Newton’s second law of motion, on any self propelling body (fish, squid, aircraft, walking man) moving with a constant velocity, the net force and the net moment acting on the body are zero. For example, on an aircraft (figure 4a), the total **lift** (L) balances the weight, and the thrust balances the aerodynamic **drag**. (For natural systems, often, there are small periodic changes in velocity superposed over a constant value. In such cases, force and moment balance can be taken as an average over one period.) As mentioned earlier, in the case of aquatic organisms, weight is roughly balanced by buoyancy force of the water. In the horizontal plane, all the forces are due to interactions of the body surface and the water and can be written as integrals of the (normal) pressure and tangential viscous shear stress over the surface (fig. 4 (inset)). (At low Reynolds numbers ($Re \ll 1$), the *normal* viscous stresses may also be significant.)

$$\vec{F} = \iint_A (P\hat{n} + \vec{F}_r) dA \quad (1)$$

Lift and Drag: Lift force is defined as the force generated on a body in the direction *normal* to the local flow direction. For example, lift on an aircraft’s wing balances most of its weight.

Drag force is the force on a body in the same direction as the flow. It is usually caused by viscous effects.

Figure 3: Schematic of a squid that uses pulsed water jet for locomotion. The water jet is pushed out through the funnel by squeezing of the mantle. The internal body cavity is then refilled with water through ducts surrounding the head, and the whole sequence is repeated periodically.

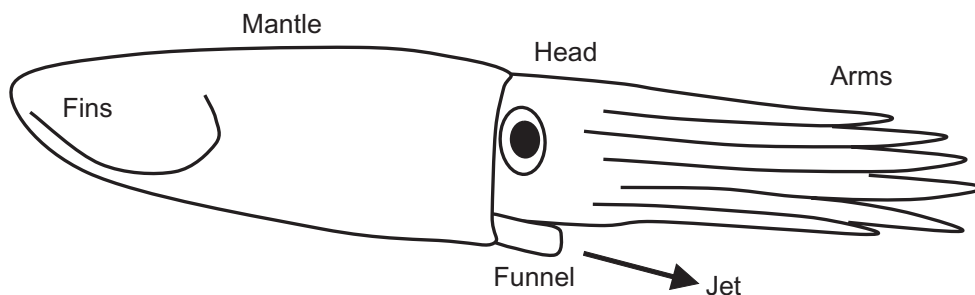
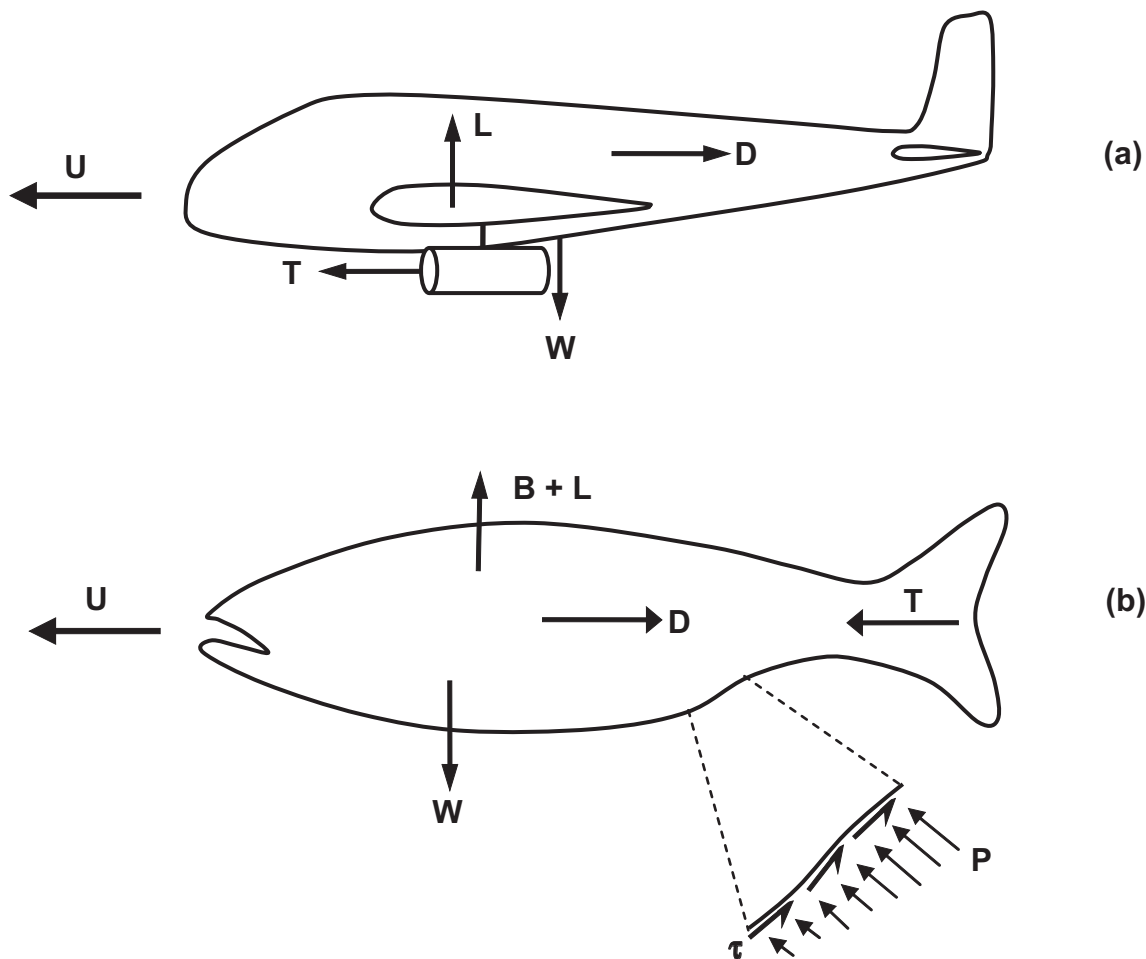


Figure 4: Schematic showing forces acting on an aircraft flying at constant speed in (a), and on a fish moving at constant speed in (b). In (a), the thrust generated by the engine (T) is equal to the drag (D) on the aircraft, while the lift force generated by the wings (L) balances the weight (W). In (b), the thrust is mainly generated by the flapping tail, while the buoyancy (B) and lift balances the weight. The fluid surface forces like lift, drag and thrust on the body are caused by the pressure (P) acting normal to the surface and the shear stress (τ) acting tangential to the surface, as shown in the inset to the figure.



where P is the pressure acting normal to the surface (\hat{n}) and \vec{F}_τ is the local force per unit area due to viscous stress, which is more typically written in tensor form.

At high Reynolds numbers, in the absence of flow separation, often it is possible to determine the velocity field from **inviscid potential flow theory** and the viscous stress from **boundary-layer theory** (Batchelor, 1967). Laplace's equation, $\nabla^2 \phi = 0$, governs the flow outside of the boundary layer, where ϕ is the velocity potential and fluid velocity $\vec{u} = \nabla(\phi)$. In the inviscid part of the flow, pressure (P) is related to velocity (U) and fluid density (ρ) through the unsteady Bernoulli equation (Batchelor, 1967):

$$\frac{\partial \phi}{\partial t} + \frac{P}{\rho} + \frac{U^2}{2} = \text{Constant} \quad (2)$$

(The usual gravity term has been left out, as it can be absorbed in the pressure term.) The last term is the familiar term, higher velocity leading to a lower pressure; for example, lift on an airfoil may be explained from the lower pressure (higher velocities) on the top surface compared to the higher pressure (lower velocities) on the lower surface. In high Reynolds number flows, forces like lift and drag scale as $(\rho U^2/2)$ times the surface area. Thus, forces are about a thousand times larger in water compared to air for the same velocity.

The first term, $\frac{\partial \phi}{\partial t}$, occurs due to unsteadiness in the flow, and is related to the added mass effect discussed in Box item 1. This term, more often than not is non-negligible in most forms of aquatic propulsion, in particular, as we shall see below, in pulsatile jet propulsion and anguilliform swimming. It can be usefully thought as arising from the fact that any motion of a solid surface, for example, the tail fin, causes the surrounding fluid to move. The acceleration of this surrounding fluid mass, termed added or virtual mass (see Box item 1), comes from the pressure associated with the $\frac{\partial \phi}{\partial t}$ term.

In most man-made systems, such as a submarine or an aircraft, the drag force which opposes the motion is mostly due to viscous stress, and usually to a much smaller extent due to pressure on the surface of the hull of the submarine or the fuselage of the aircraft. The thrust from a propeller or a jet engine overcomes the drag force (figure 4(a)). There is little interaction between the drag producing part (the main body) and thrust producing parts and they may be treated and analysed as separate entities. A second characteristic of man-made self propelling systems is that the flow (for the constant velocity case) is essentially steady; pressure on the hull or fuselage

surface and on the propeller blades are from the $\rho U^2/2$ term in the Bernoulli equation.

In contrast, for systems found in nature, it is many times difficult or even impossible to distinguish between thrust producing and drag producing components; for the fish shown schematically in figure 4(b), even though it is shown that the tail produces the thrust and the rest of the body experiences drag, this is generally not the case, as will be discussed in the sections below. And invariably the flow is unsteady. Pressure due to the inertia or added mass of the fluid on the oscillating caudal fin of a shark or on the undulating body of an eel forms an important component of the overall force balance. A more subtle and perhaps equally important effect is that of unsteadiness on the boundary layers. How different are the boundary layers on an undulating, flexible fish body and those on a rigid steadily moving submarine? Does the unsteadiness enhance the turbulence or suppress it, increase the viscous friction or reduce it? These two features—no clear distinction between thrust and drag and the flow unsteadiness—make the study of the hydrodynamics of aquatic propulsion both interesting and challenging.

3. Anguilliform Mode of Swimming

Anguilliform swimming, most commonly seen in eels, is characterized by undulation of the whole body, with the amplitude of undulation increasing from head to tail. The earliest studies were by Gray (1933), who made detailed measurements of the kinematics of eel motion, and also proposed possible mechanisms of propulsion. Detailed quantitative information has been recently obtained from both particle-image velocimetry (PIV) measurements around swimming eels in a water tunnel (Tytell & Lauder, 2004; Tytell, 2004) and 3-d computations of the flow (for example, Kern & Koumoutsakos, 2006). Figure 5 reproduced from Gray's paper, shows the undulation of the body over one cycle.

The undulation is best described as a wave moving down the body with a phase velocity V (figure 6)

$$z = h(x - Vt) \quad (0 < x < l) \quad (3)$$

Here, l is length of the body and h is the lateral displacement. At a fixed x , the body oscillates laterally with frequency, $f = V/\lambda$, where λ is the wavelength. In this type of locomotion, typically, one and half waves are seen along the length of the body. We will see below that thrust from such

Inviscid Potential flow theory: The flow field is represented as the gradient of a scalar potential, $\vec{u} = \nabla(\phi)$ and the governing equation is the linear Laplace's equation $\nabla^2 \phi = 0$, which is relatively easy to solve. This theory is very useful in high Reynolds number flows, and is applicable to the region outside the viscous boundary layers.

Boundary layer theory: In high Reynolds number flows, the viscous effects are confined to thin regions near the body referred to as boundary layers. Within these regions, simplifying assumptions can be made such as the fact that gradients across the thin boundary layers are much larger than gradients along the boundary layer, enabling a simplified boundary layer theory. Proposed by Prandtl in 1904, boundary layer theory revolutionized study of fluid mechanics, and also led to the development of singular perturbation theory widely used in applied math and physics.

Box Item 1: Added Mass

A body moving in fluid (with speed U_b) ‘carries’ some of the surrounding fluid along with it. The momentum and kinetic energy associated with the motion of this surrounding fluid may be written as $m_a U_b$ and $m_a U_b^2/2$ respectively; m_a is termed as the added or virtual mass. Thus, if the body accelerates, the surrounding fluid will also accelerate along with it, and the force on the body (in addition to the drag) may be written as

$$F = -(m_b + m_a) \frac{d(U_b)}{dt}$$

Thus a body *accelerating* in a stationary fluid experiences a force resisting the acceleration, in addition to one due its own mass, m_b .

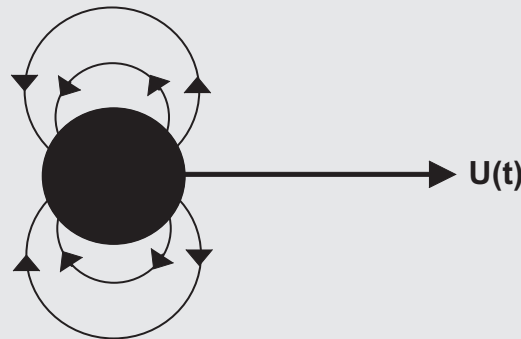
For inviscid, potential flow, added mass may be calculated exactly. This resistive force on an accelerating body can be computed by integrating the pressure around the body, with the pressure being determined using the unsteady Bernoulli equation and the unsteady potential for the flow around the body.

The streamlines for inviscid flow around a moving cylinder (figure B2) show that fluid from the front of the body has to be accelerated and moved to the rear to make way for the accelerating body. In the above case, the displaced fluid mass, m_d , would be referred to as “added mass” in the sense that this additional mass of fluid also needs to be accelerated in order for the body to accelerate.

The added mass values for arbitrary body shapes (2D and 3D) computed from potential flow are tabulated in many books (Newman, 1977; Blevins, 2001). For a circular cylinder, $m_a = 1.0 * m_d$, and for a sphere, $m_a = 0.5 * m_d$, where m_d is the mass of the displaced fluid. In general added mass is a tensor, and depends on the direction of acceleration of the body; added mass of a circular disc moving in its own plane is zero.

Added mass forces are very important for bodies moving in water, such as fishes, as the added mass is usually comparable or may even exceed the body mass. However, in air, added mass forces are usually negligible as the body mass is typically much larger than the added mass that scales with the displaced fluid mass; however, for airships and balloons, added mass effects are important.

Figure B1: Streamlines for a circular cylinder moving with velocity $U(t)$ in a stationary fluid.

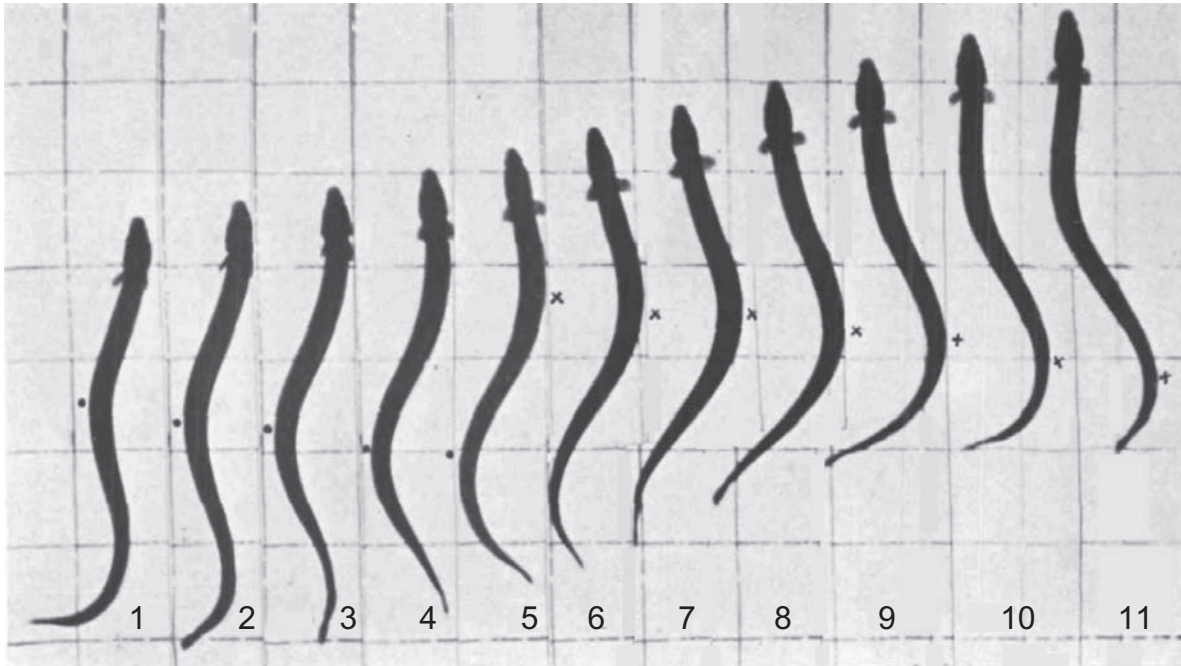


a wave is only possible when $V > U_b$, where U_b is the steady forward swimming body velocity.

Two types of theories have been proposed to explain anguilliform swimming, resistive and reactive. The resistive theory, which works well at low Reynolds numbers, seems to be less suited at the high Reynolds numbers, and is based on the difference in the resistive forces that a longitudinal element of the body experiences in tangential and

normal directions. Reactive theories, primarily developed by Lighthill and Wu (Lighthill, 1960; Lighthill, 1975; Wu, 1961; Wu, 1966), are based on the force required on each element of the body to add momentum (and energy) to the fluid mass (the added or virtual mass) surrounding that element. The slender body, inviscid potential flow theories of Lighthill and Wu (see Wu 2011) give insight into the force generation mechanism.

Figure 5: Successive pictures of a swimming eel from Gray (1933). Reproduced with permission from the Company of Biologists (J. Gray (1933), "Studies in Animal Locomotion: I. The Movement of Fish with Special Reference to the Eel", J Exp Biol, 10, 88-104.) The successive pictures are taken at time intervals of 0.05s and show the progression of the body wave backwards, as marked by the dots and crosses, to propel the eel forward.



For a body moving forward with constant velocity U_b , the slender body theory gives the following relations for power required (P), rate of kinetic energy added to the fluid (E) and thrust (T):

$$\begin{aligned} \bar{P} &= mU_b \left\{ \overline{\frac{\partial h}{\partial t} \left(\frac{\partial h}{\partial t} + U_b \frac{\partial h}{\partial x} \right)} \right\}, \\ \bar{E} &= \frac{m}{2} U_b \left\{ \overline{\left(\frac{\partial h}{\partial t} + U_b \frac{\partial h}{\partial x} \right)^2} \right\} \text{ and} \quad (4) \\ \bar{T} &= \frac{m}{2} \left\{ \overline{\left(\frac{\partial h}{\partial t} \right)^2} - U_b^2 \overline{\left(\frac{\partial h}{\partial x} \right)^2} \right\} \end{aligned}$$

Here, m is the added mass per unit length = $\rho\pi b^2$, where $2b$ is the width of the body. The overbar represents average taken over one time period, and the averages are evaluated at $x = l$, at the tail. For a waving ribbon plate of width, $2b$, length l , wave speed V , these relations reduce to

$$\begin{aligned} P &= mU_b V (V - U_b) \overline{h_x^2}, \quad E = \frac{m}{2} U_b (V - U_b)^2 \overline{h_x^2}, \\ T &= \frac{m}{2} (V^2 - U_b^2) \overline{h_x^2} \end{aligned} \quad (5)$$

Clearly, positive thrust is obtained only when $V > U_b$. Note also the dependence on the average of the slope squared (h_x^2) for the three quantities; this average is proportional to $(A/l)^2$, where A is the amplitude of oscillation of the tail.

The input power (P) goes into kinetic energy of the fluid (E) and for doing useful work (TU_b):

$$P = E + TU_b \quad (6)$$

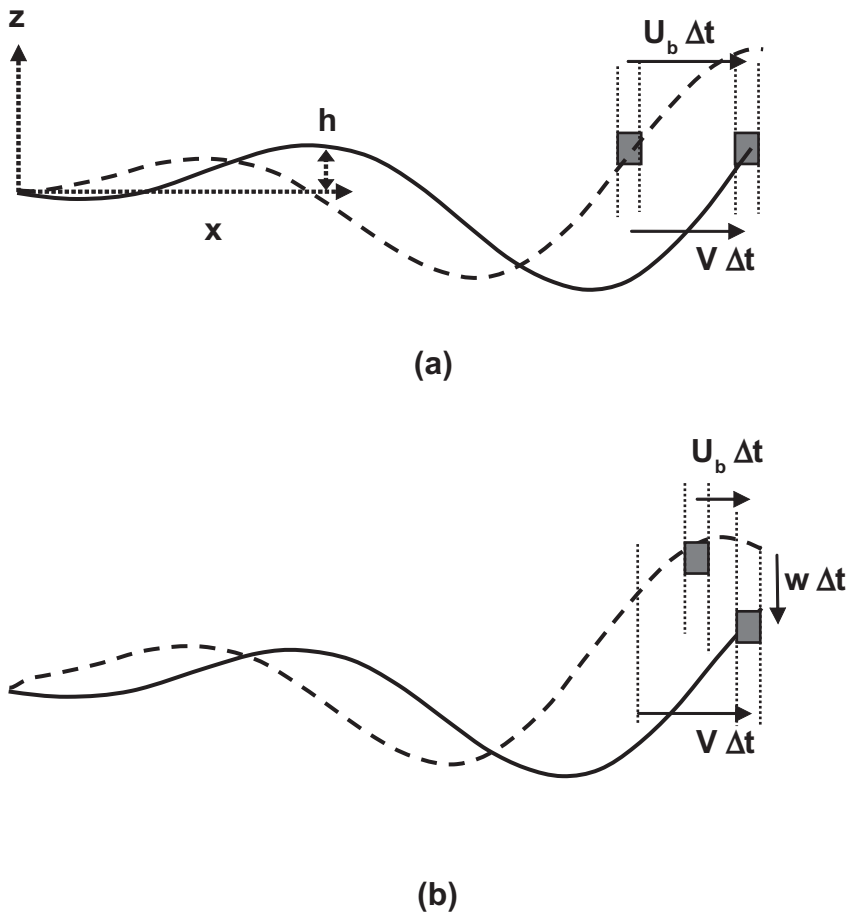
The hydrodynamic propulsive efficiency may then be defined as the ratio of useful work to total input power:

$$\eta = \frac{TU_b}{P} = \frac{V + U_b}{2V} = \frac{P - E}{P} = 1 - \frac{V - U_b}{2V} \quad (7)$$

This efficiency approaches unity, as V tends to U_b .

This theory, though inevitably less rigorously, has been extended to large amplitudes by Lighthill (Lighthill, 1971). A key result from these theories is that thrust and work done are related to time averages of the kinematic quantities at the tail end; motions in the posterior side do not seem to matter. Physically, the thrust generation may be understood from figure 6. In figure 6(a),

Figure 6: Schematic for the reactive theory of Lighthill as applied to an eel. In both (a) and (b), the continuous curved line represents an eel idealized as a travelling wave at an instant (t), while the dashed line represents the same travelling wave (or eel) at a slightly earlier time ($t - \Delta t$), with the wave speed V being the same in both cases. In (a), the eel body velocity U_b is the same as the wave speed (V), which means that the fluid shown as the shaded area on the continuous line would have moved along with the wave and will have no lateral velocity. On the other hand, in (b), the fluid velocity (U_b) is smaller than the wave speed (V), and the shaded fluid would have been pushed downwards from the earlier instant with lateral velocity (w), as shown.



when the wave speed and fluid velocity are same, a fluid particle, shown shaded, will move with the wave without any lateral displacement. However, when the wave velocity is larger than the fluid velocity (figure 6b), the fluid particle gets displaced downwards by the body motion, and correspondingly work done is done by the fish on the fluid. Component of the reaction force in the forward direction provides the thrust. A net thrust is generated only in the tail region; elsewhere the forces cancel over one cycle.

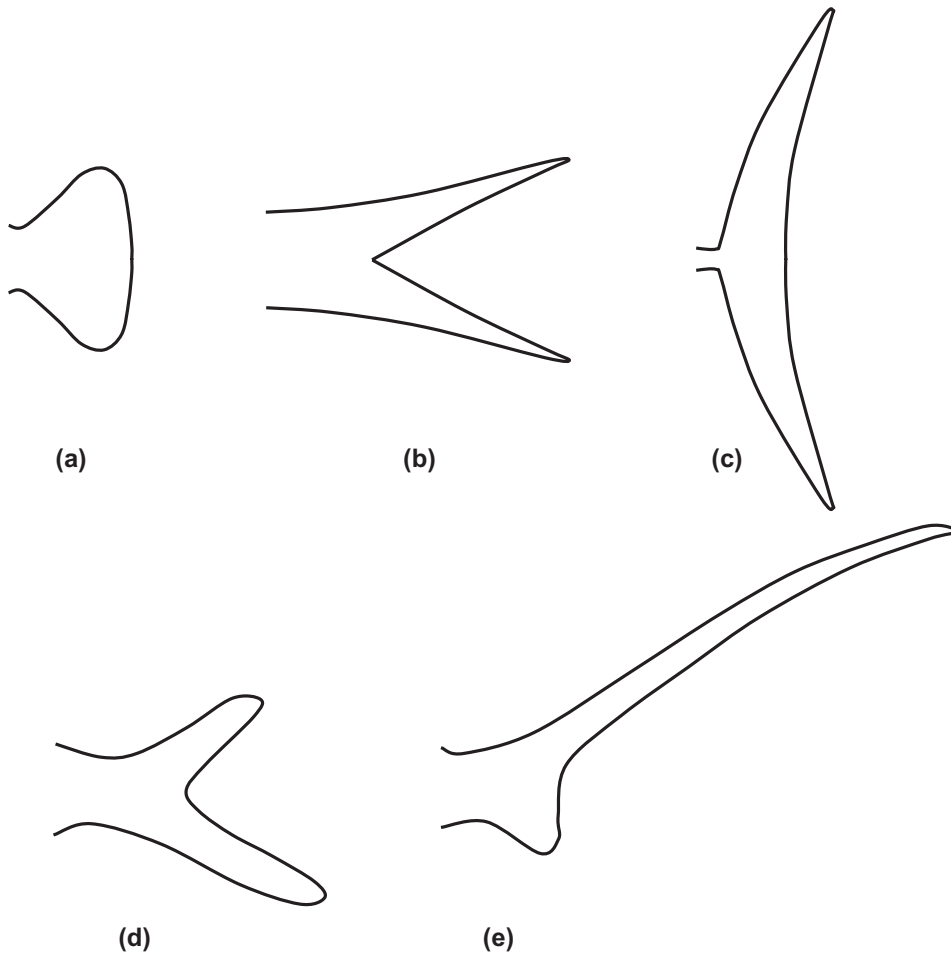
4. Thunniform Mode of Swimming

In contrast to the anguilliform mode, in the carangiform and thunniform modes, the undulation over most of the body length is small,

and is largest only at the anterior (tail) end. The caudal fin in these types of fish seems to generate most of the thrust which overcomes the drag force on the rest of the body. A variety of tail forms are seen in such swimmers (figure 7).

Understanding and analyzing thrust generation is easiest done for thunniform swimmers who have the *caudal fin in the shape of a high-aspect-ratio, swept-back wing* (figure 7c), which is often termed as the lunate tail; the lunate tail is characteristic of many high speed fish like dolphins and some sharks. The lunate tail and rest of the body are connected through a narrow region called the peduncle. The thrust producing and drag producing parts are reasonably distinct, as in a submarine. And in both cases thrust is

Figure 7: Different types of fish tails (caudal fins). Symmetrical tails such as in (a) and (b) above are referred to as homocercal tails. These can have low aspect ratio ($AR = S^2/A$, where S is the maximum height of the tail and A is the surface area), as in (a) and (b), or have a large aspect ratio as in (c); the latter being a preferred form for high-speed swimming, while the former is useful for high maneuverability. Although the AR is similar in (a) and (b), their shapes are very different with (b) having a forked shape as shown in figure 2 for a silver shark. Non-symmetrical tails are referred to as heterocercal and are shown in (d) and (e). When the lower part is extended, as in (d), it is referred to as hypocercal and is useful in flying fishes such as the atlantic flying fish to generate thrust during takeoff when the body is already outside water. On the other hand, when the upper part is extended, it is referred to as epicercal and this kind of tail generates a vertical force in addition to thrust. Adapted from Videler (1993).



from lift generated by the airfoil cross-section, of the propeller in a submarine or of the caudal fin in a thunniform swimmer. Of course, a propeller produces a steady thrust and no side force, whereas the flapping caudal fin produces a periodically varying thrust as well as side force.

Both man and nature have converged to the airfoil shape, a remarkable device to produce a large lateral force (lift) compared to the drag force. The airfoil forms the basis for a large number of surfaces where lift or thrust needs to be produced efficiently. Wings of aircraft and birds, propeller and helicopter rotor blades, tails of fish (figure 8b) all have cross sections with an airfoil shape.

The lift force (L) is usually written as:

$$L = C_L \left(\frac{1}{2} \rho U_r^2 \right) A_s \quad (8)$$

where C_L is the lift coefficient, U_r is the velocity of the fluid *relative* to the foil, and A_s is the planform area of the foil. For symmetrical airfoils of the type found in fish tails, the lift coefficient $C_L \approx 2\pi\alpha$, where α is the angle of attack between the airfoil and the relative velocity direction. The lift coefficient is typically around 1. Another useful way of representing lift is in terms of bound circulation (Γ) (see box item 2) around the airfoil and the relative velocity (U_r).

Box Item 2: Vorticity, Circulation and Vortex Rings

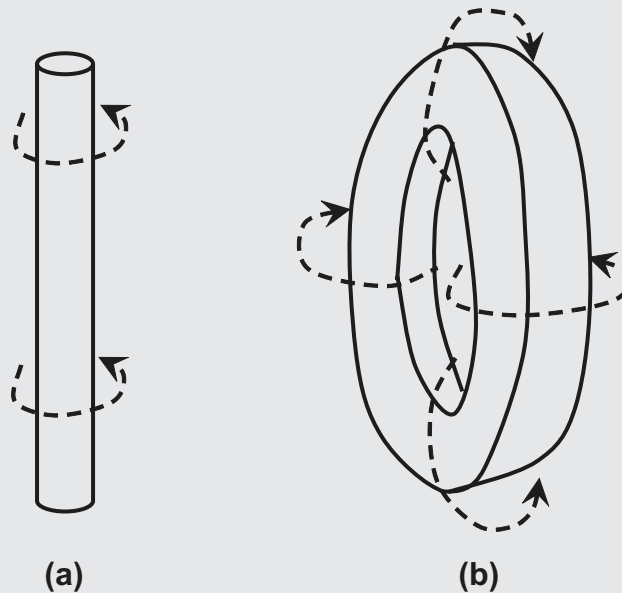
In fluid flows, especially at high Reynolds numbers, it is very useful to think of a quantity called the vorticity (ω), which like velocity is a vector, and is defined as the curl of the velocity field (\mathbf{u}), $\omega = \nabla \times \mathbf{u}$ (Batchelor, 1967). Vorticity can be shown to be twice the angular velocity of a spherical “fluid particle”. In most flows, vorticity is generated at solid surfaces, due to the no-slip boundary condition at the surface. The vorticity thus generated is convected in to the bulk of the flow.

At high Reynolds numbers, we have boundary layers near surfaces, which are regions of large velocity gradients and thus large vorticity. Boundary layers coming off sharp edges, like that of a fin, often roll up into vortices. Vortices are concentrated regions of vorticity with local streamlines that are circular; concentrated swirls, such as those in hurricanes and whirlpools are vortices. Hurricanes may be considered as line vortices, in that vorticity is concentrated in thin “vortex cores,” with long axial length.

Vortex rings are toroidal or donut shaped vortices, a line vortex that is bent with the two ends being joined. Every time, we blow, say smoke, out of our mouths, a vortex ring forms. Such vortex rings are very common in nature ranging from flows in human hearts to fish wakes.

Circulation (Γ) is the strength of a vortex. It can be computed as the area integral of the vorticity over the vortex cross-section, $\Gamma = \int \omega dA$. Using Stokes theorem, the circulation may also be equivalently computed as the line integral of the fluid velocity around a closed loop, $\Gamma = \oint \vec{u} \cdot d\vec{l}$. In the case of a line vortex, like a hurricane, and a vortex ring, the circulation would necessarily be the same at every cross-section (Batchelor, 1967). Momentum and kinetic energy in fluid flow are often written in terms of vorticity and circulation.

Figure B2: (a) A line vortex like a hurricane. (b) A vortex ring. In both cases, the sense of rotation of the fluid is shown by the arrows.



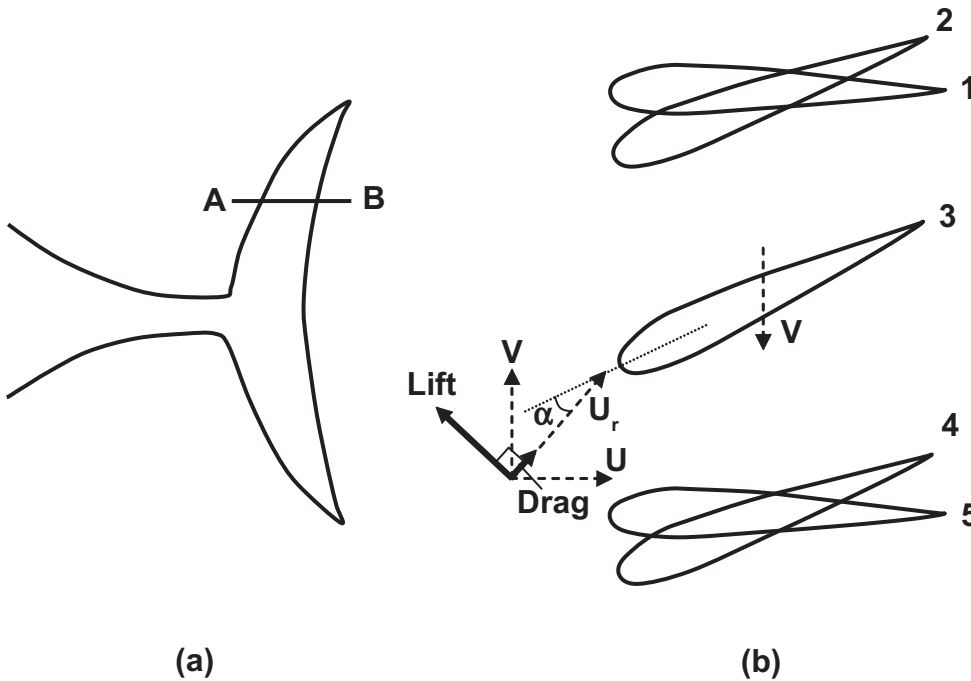
$$L = \rho U_r \Gamma \tag{9}$$

To produce lift efficiently, i.e., without flow separating from the airfoil surface, the angle between the airfoil and the flow relative to it, the angle of attack (α), must be less than the stall angle of about 12 to 15 degrees. An appropriate angle of attack is maintained in the propeller by the twist in the blade, and in the fish by continuous rotation of the caudal fin as it flaps back and forth (see figure 8b).

Side to side motion of an airfoil is termed as heaving motion, and rotation of the airfoil is termed as pitching motion. It has been shown (Anderson et al., 1998) that most efficient thrust production is achieved when there is both heaving and pitching with a certain phase difference between these two motions. The lunate tails of thunniform swimmers seem to have achieved this optimum motion.

No doubt, both the thrust generating mechanisms of the anguilliform mode and the

Figure 8: (a) The cross-section (AB) of the fish tail is a symmetric foil. (b) Top view of the cross-section AB showing the motions of the foil in time (1 to 5), representing half a cycle of tail flapping. As the fish flaps its tail from side to side, the airfoil moves laterally (heave) and also rotates about an axis (pitch). The lift and drag forces, shown by the dark thick lines, are perpendicular and parallel to the resultant speed (U_r) of the foil, which is due to both the forward speed (U) of the fish and the lateral speed (V) of the fish tail. The lift force is mainly dependent on the angle of attack (α) of the foil, which is the angle between the foil and the resultant speed (U_r) of the foil. (Adapted from Lighthill, 1986.)



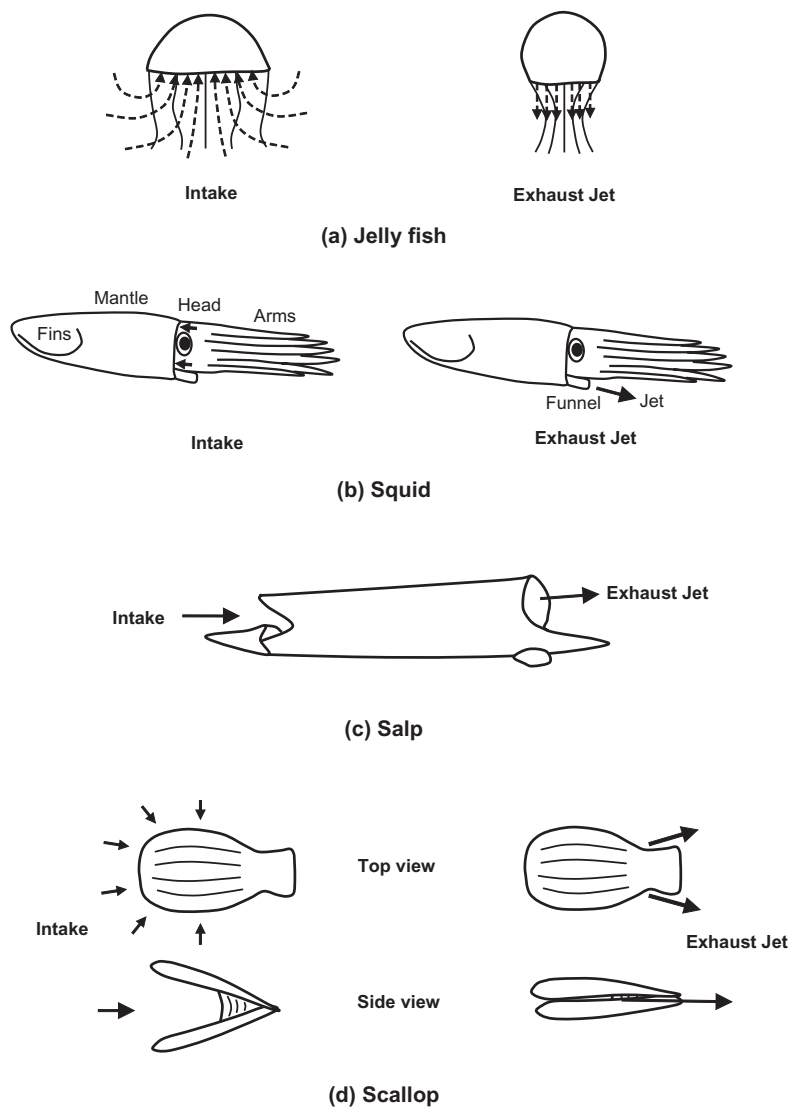
thunniform mode are present in all fishes having the undulatory swimming motions shown in figure 1, with only the relative contributions changing. In particular the caudal fins shown in figure 7(a, b) will probably have both components of thrust generation in almost equal measure. Because of the unsteady nature of the flow, even a lunate tail will experience a reactive force, of the type found in the anguilliform mode, in addition to the lift. Asymmetrical shaped tails (figure 7d, e) produce a vertical force in addition to the thrust. In, for example, the fin shown in figure 7e found in some sharks, a longitudinal wave passes along the length of the tail, to produce the upward force.

5. Pulsed Jet Propulsion: Squid and Salp Type

As seen in the previous sections, fishes broadly locomote by periodic lateral undulatory motions of their bodies and fin in both the thunniform and the anguilliform mode. In contrast to this, there are many species of aquatic creatures that locomote using pulsed jets. These creatures in general take in water through an inlet in to a portion of the body,

and then send out a well directed jet of water in a direction opposite to the required direction of motion. The resulting jet thrust propels the body forward, and the whole sequence of water intake and jetting is repeated in a periodic manner. This mechanism of propulsion and locomotion is quite different from the undulatory motions of the fish and hence the morphological characteristics of these creatures are quite different from fishes. Figure 9 shows some aquatic creatures that use such a propulsion mechanism and each of them has features that are quite distinct. The simplest among them is perhaps the jellyfish (figure 9(a)), which uses the same orifice in its body for intake and for expelling the water; by expanding the “bell”, water is drawn in to the umbrella like cavity, and then expelled out by contraction of the same bell. The squids (figure 9(b)) have a range of propulsion options including fins on their mantle that are used at low speeds, their arms that can be used to move around rocky underwater terrain and pulsed jets that are almost purely the source of propulsion at high speeds (Bartolo et al., 2001). For the pulsed jets, squids take in water through ducts between the mantle

Figure 9: Aquatic creatures that locomote using pulsed jets. (a) Jellyfish take in and exhaust a water jet from the same body orifice by expanding and contracting the umbrella like “bell”. The flow path during intake and exhaust is shown by the dashed lines. (b) Squids take in water through ducts between the mantle and head and send out a pulsed jet through a funnel; these actions being driven by expansion and contraction of the mantle. (c) Salps are unique in that they have two separate orifices, one in front for intake and the other in the rear for the jet exhaust. The intake and exit orifices are used for a number of functions including respiration, food and propulsion. Among the creatures that use pulsed jet propulsion they are generally thought to be the most efficient. (d) Scallops consist essentially of two shells with an abductor muscle between them. During the intake phase, the shells are apart and water is drawn in from the surroundings. The muscle then pulls the shells together before the exhaust jets are sent out from two rear orifices.



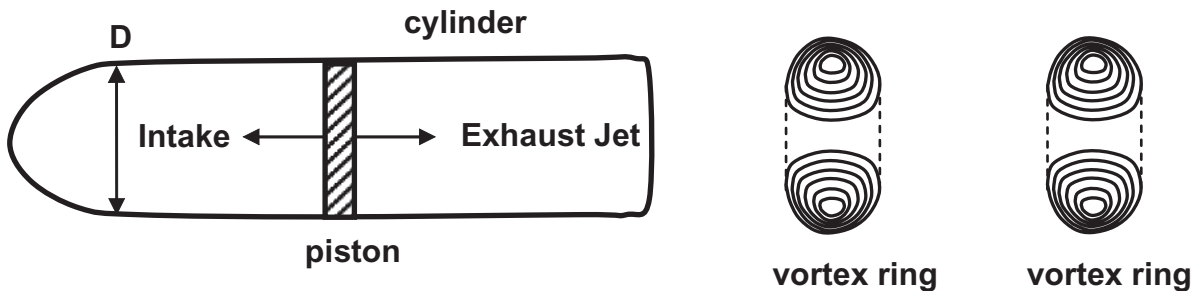
and the head, then close these openings, followed by contraction of the mantle cavity to squeeze out a high speed jet through a “funnel” whose direction can be changed to achieve controlled motion. Salps

(figure 9(c)) perhaps come closest to a “jet engine”, to be more precise a pulsed jet engine, taking in water from the front of their bodies, pumping it backwards through their bodies and pushing out the water through a rear opening. In the case of the salps, this flow through the body besides providing thrust also provides “chemosensory information, food, respiratory gas exchange, removal of solid and dissolved wastes, dispersal of sperm” (Madin, 1990). Scallops (figure 9(d)) are morphologically quite different from the others, and also locomote using pulsed jets.

Although there are large variations within the aquatic creatures mentioned above, a common and important point in all of them is a transient or pulsed jet of water to create thrust, followed by a suction phase where the water is taken in to the body cavity. An idealization of this system that has been studied extensively in the fluid mechanics community is a piston-cylinder arrangement shown schematically in figure 10. As the piston moves to the right inside the cylinder, it pushes out fluid from the open right end of the cylinder forming a water jet. This water jet coming out of the cylinder contains boundary layer vorticity (Box item 2), which eventually rolls up to form a vortex ring (a “smoke” ring in water) as shown in the schematic. In this simple idealization of a pulsed jet based aquatic creature, the intake occurs as the piston is moved back to its original position (leftwards). Periodic back and forth motion of the piston produces a train of vortex rings as shown in figure 10.

The formation of vortex rings from a piston-cylinder arrangement has been studied extensively (e.g. Didden, 1979; Gharib et al., 1998). The circulation of the generated vortex ring, a measure of its strength (Box item 2), has been studied for example as a function of the normalized stroke length (L_p/D_p , where L_p is the piston stroke and D_p is the cylinder diameter). For small normalized stroke length (L_p/D_p), a vortex ring is formed as shown in figure 11(a) (from Gharib et al., 1998), with all the vorticity and mass being entrained in to the vortex ring. With increase in piston stroke (L_p/D_p), the circulation and size of the vortex ring increases. However, beyond a certain L_p/D_p , the vortex ring size cannot increase further, and the additional fluid and vorticity is contained in a “trailing jet” that is disconnected from the vortex ring as seen in figure 11(c). The vortex ring is then said to have “pinched off”. The largest value of the normalized stroke length at which only the ring forms without a trailing jet is referred to as the “formation number” and was found to be about 4 (Gharib et al., 1998). At this L_p/D_p value, the strongest vortex ring is formed with no trailing

Figure 10: An idealized model of an aquatic organism using pulsed jets for locomotion. In this model, the “organism” consists of a piston-cylinder arrangement with the rear end of the cylinder being open. As the piston moves to the right within the cylinder (of diameter D_p) by a normalized stroke length (L_p/D_p), fluid is pushed out through the rear open end, resulting in the formation of a vortex ring. Intake occurs as the piston moves to the left within the cylinder, and the whole process is repeated periodically, with a vortex ring being generated in each cycle. The resulting thrust would propel the “organism” to the left in this case.



jet, as shown in figure 11(b). Beyond this critical value, further increase in L_p/D_p does not change the strength of the leading vortex ring and all additional vorticity is left in the disconnected trailing jet. The largest vortex ring formed may be understood by the elegant analysis of Linden and Turner (2001). They showed using a simplified model vortex ring (Norbury, 1973) that the limiting vortex ring formed is the largest single vortex ring that may be formed while conserving circulation, impulse, volume and energy between the ejected “plug” of fluid and the vortex ring formed. They hence suggest that the limiting vortex is “optimal” in the “sense that it has maximum impulse, circulation and volume for a given energy input.”

A simple equation representing the average thrust produced in one stroke by a piston cylinder arrangement can be obtained from a control volume analysis. The average thrust force (T) is given by:

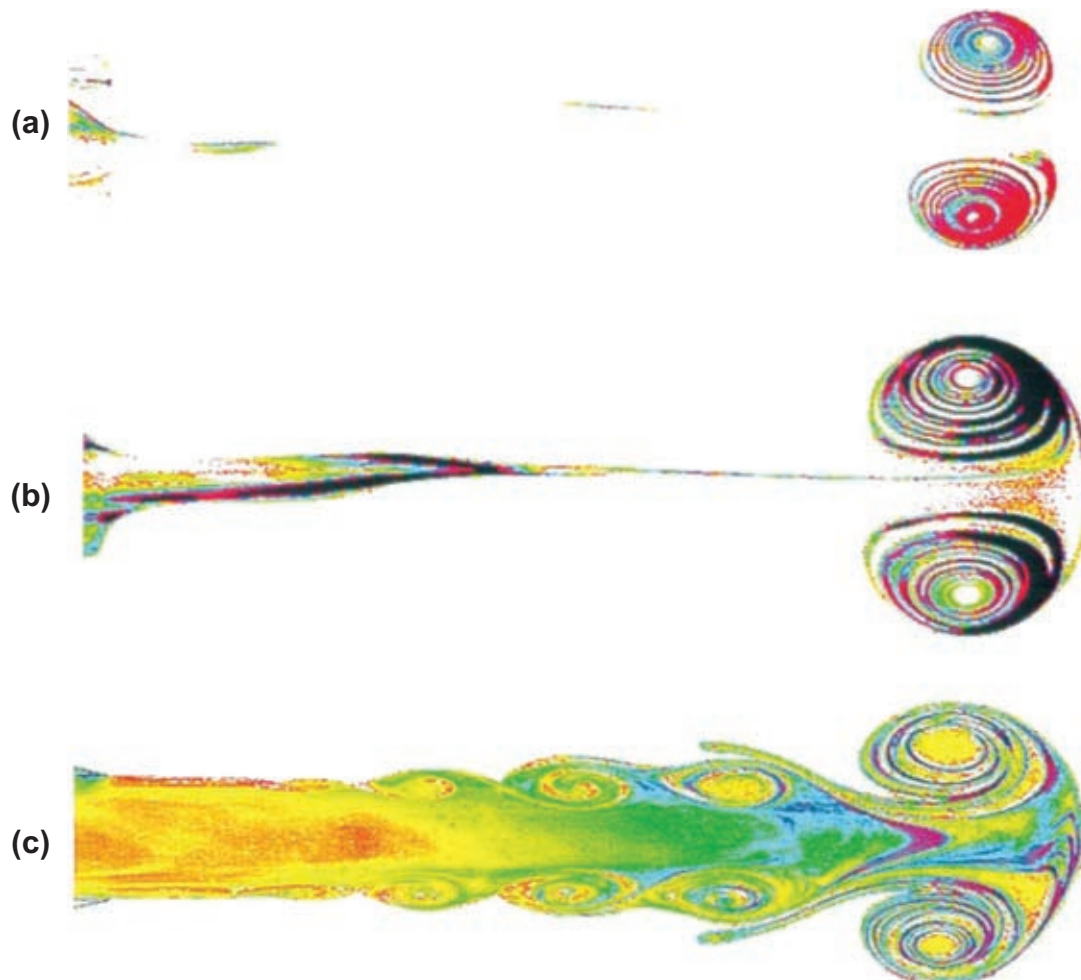
$$T = \frac{1}{T_s} \int_0^{T_s} \int_A \rho u_j^2 dA dt + \frac{1}{T_s} \int_0^{T_s} \int_A (P_e - P_\infty) dA dt \quad (10)$$

where ρ is the fluid density, u_j is the jet velocity at the cylinder exit, P_e is the pressure at the exit plane, P_∞ is the pressure far away from the body, A is the cross-sectional area of the cylinder/jet and T_s is the time period for one stroke. The average thrust (F_T) has two components, the first term representing the outward jet momentum that in its simplest form would be the product of mass flux and the jet velocity ($\dot{m} u_j$), while the second term represents the difference in pressures at the exit plane (P_e) and in the ambient (P_∞), the so

called “over-pressure” (Krueger & Gharib, 2003). In the case of a steady jet, only the first term is non-zero, as the pressure at the exit plane is the same as the pressure far downstream. In the unsteady case, both terms contribute to thrust and it is important to account for the second term as well, as shown by Krueger & Gharib (2003). The over-pressure is due to the fact that ambient fluid just outside the exit has to be accelerated and moved out of the way during the ejection phase. Overpressure can be calculated in potential flow using the unsteady form of the Bernoulli equation and is linked directly to the concept of “added mass” (Box item 1). Krueger and Gharib (2003) directly measured the thrust force on a piston-cylinder arrangement for varying piston stroke lengths (L_p/D_p). They found that the maximum average thrust (F_T) is obtained at $L_p/D_p \approx 4$, which represents the stroke length giving the largest single vortex ring. Their measurements showed that the over-pressure provided 42% additional thrust, but only during the vortex ring formation phase. This mechanism of thrust generation is essentially not present during the ejection of the trailing jet, where the flow becomes more like a steady jet. This line of thinking has resulted in a view that for efficient thrust generation, it is ideal to eject “Optimal” vortex rings, which appear to form at normalized stroke lengths (L_p/D_p) of about 4 (Linden & Turner, 2004; Dabiri, 2009).

It is important to note that at the large Reynolds numbers associated with these flows, the streamlines for the jet flow outwards and the in-flow back to the cylinder would be completely different, as schematically illustrated in figure 12. In the inflow case, the flow would come in from all directions, while in the outflow case this

Figure 11: Visualization of the flow and vortex ring formed due to a single stroke of a piston inside a cylinder from Gharib et al. (1998). Reproduced with permission from Cambridge University Press (M. Gharib, E. Rambod, K. Shariff (1998), "A universal time-scale for vortex ring formation", *Journal of Fluid Mechanics*, 360, 121-140.) In (a), the normalized stroke length (L_p/D_p) is 2, and all the vorticity from the inner wall of the cylinder ends up in the vortex ring. In (b), the L_p/D_p is 3.8, close to the "formation number", and the vortex ring strength or circulation has grown to about its maximum value. In (c), $L_p/D_p = 14.5$, much larger than the formation number, and the vortex ring strength is about the same as in (b), with the additional vorticity from the cylinder ending up in a "trailing jet" that is separated from the vortex ring. Case (b), where L_p/D_p is close to the formation number, may be considered to be the optimal piston stroke from the thrust generation point of view.

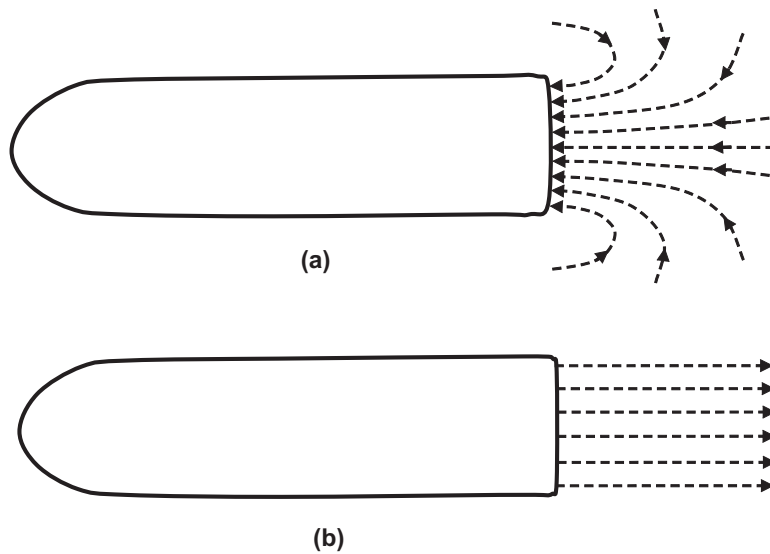


symmetry is broken as the viscous boundary layer coming out of the inner cylinder wall cannot turn around the sharp corner at the end of the tube, thus leading to boundary layer separation and hence straight streamlines, as seen for example in flow out of a car exhaust. The difference in inflow and outflow implies that a cyclically run piston would in each outward-stroke form a vortex ring, and in the inward refilling stage take in water from the surroundings leaving a train of vortex rings. Very similar type of flow occurs for example in the putt-putt boat (Sharadha & Arakeri, 2004), during human breathing through

nostrils, and in a "synthetic jet" (Glezer & Amitay, 2002) that is used in flow control applications. For pulsed-jet propelled organisms, the thrust force, discussed earlier, would only be generated during the ejection phase, with the intake phase providing either no thrust or small negative thrust, for example in the case of a jellyfish.

There have been several detailed studies on aquatic creatures such as jellyfish (Colin and Costello, 2002; Dabiri et al., 2005), squids (Bartol et al., 2001; Anderson & Grosenbaugh, 2005) and salps (Madin, 1990) that locomote using pulsed jet propulsion. It is possible from these studies to

Figure 12: Streamlines during (a) intake and (b) exhaust from a cylindrical tube. In (a) during intake, the flow is taken in from all directions, while in (b), during exhaust, the streamlines come out straight from the tube due to viscous boundary layer separation at the sharp edge.



actually calculate the normalized stroke lengths (L_p/D_p) corresponding to the jet exhaust and to see if it is close to the value of 4 seen in the experiments of Gharib et al. (1998) for the formation of optimal vortex rings. From this point of view, it appears that squids are not very efficient as the effective L_p/D_p values from experimental observations suggest that it is very large, with estimated values from Johnson et al. (1972) being about 87 and that from Anderson & Demont (2000) being about 34, as reported by Linden and Turner (2004). It should be noted here that for squids the jet exhaust velocities estimated from Johnson et al. (1972) are about 6 m/s through an orifice opening of about 1.5 cm², indicating a high speed jet through a very narrow opening, resulting in very large L_p/D_p values, and that would also naturally result in large kinetic energy loss in the wake. Squids are in general thought to be very inefficient from the locomotion point of view, as seen in the statement by Videler (1993): “the squid *loligo opalescens* and heaviest sockeye salmon share approximately the same mass, optimum swimming velocity and body length, but the squid, using jet propulsion, needs more than five times as much energy.” In squids, pulsed jet propulsion appears to be designed for large acceleration, speed, and maneuverability, and not for efficient cruise. In contrast, salps have a locomotory system that provides efficient steady swimming speeds, as they do not require speed or

maneuverability. Madin (1990) estimates the L_p/D_p values for the jet exhaust from a salp to be about 6.7, not very far from the optimal value of 4. Salps also have the advantage of having unidirectional flow of water through their bodies, taking in water from the front and pushing it out through the rear, thus avoiding any significant deceleration that would be expected during the in-take phase, for example in a jellyfish.

The formation number of 4 is for rings formed in stationary fluid. It may be different due to reasons like the presence of co-flow, changes in jet velocity variation with time, and possibly the orifice diameter variation with time, as discussed by Dabiri (2009). For example, experiments by Krueger et al. (2006) for a piston-cylinder arrangement in a co-flow of velocity U_b outside the cylinder, show that depending on the ratio of U_b/U_j (U_j is the jet velocity), the formation number can vary substantially. This type of co-flow would occur in our idealized piston-cylinder organism in figure 10, during forward motion (U_b) of the body. Although, co-flow and other factors can change the value of the formation number, the basic concept of a formation number at which the vortex ring pinches off, and the fact that the corresponding vortex ring formed is “optimal” appear to be generic results that would be useful in the context of pulsed jet propulsion.

6. Momentum and Energy in the Wake

For all self-propelling bodies, some general and very useful deductions are possible from the conservation of momentum and energy principles. We have already seen that in such bodies moving with constant velocity, the net force and moment on them are zero. In the case of land-based, self-propelling bodies moving at constant velocity, the energy goes into local non-elastic deformations in the body and ground and, especially for non-steady motion, like running, into waves or vibrations in the body and the ground; of course, all the energy finally goes into heat. (If the body is accelerating, some of the energy goes into the increasing kinetic energy of the body.) There is very little effect of the motion seen in the environment. In contrast, self-propelling bodies in air and water leave definitive and revealing signatures in the fluid downstream of the body, i.e. the wake. The wake can be ‘seen’ for several 100s of the body’s lateral dimension; the wake of for example a 747/jumbo jet is particularly strong and is felt several km downstream; consequences may be disastrous for a small plane caught in its wake.

Application of the principle of momentum conservation (Prandtl and Tietjens, 1957) relates

the force on a body to the flux of momentum in the wake far enough downstream of the body:

$$F_x = \iint_A \rho(u+U_b)u dA \quad (11)$$

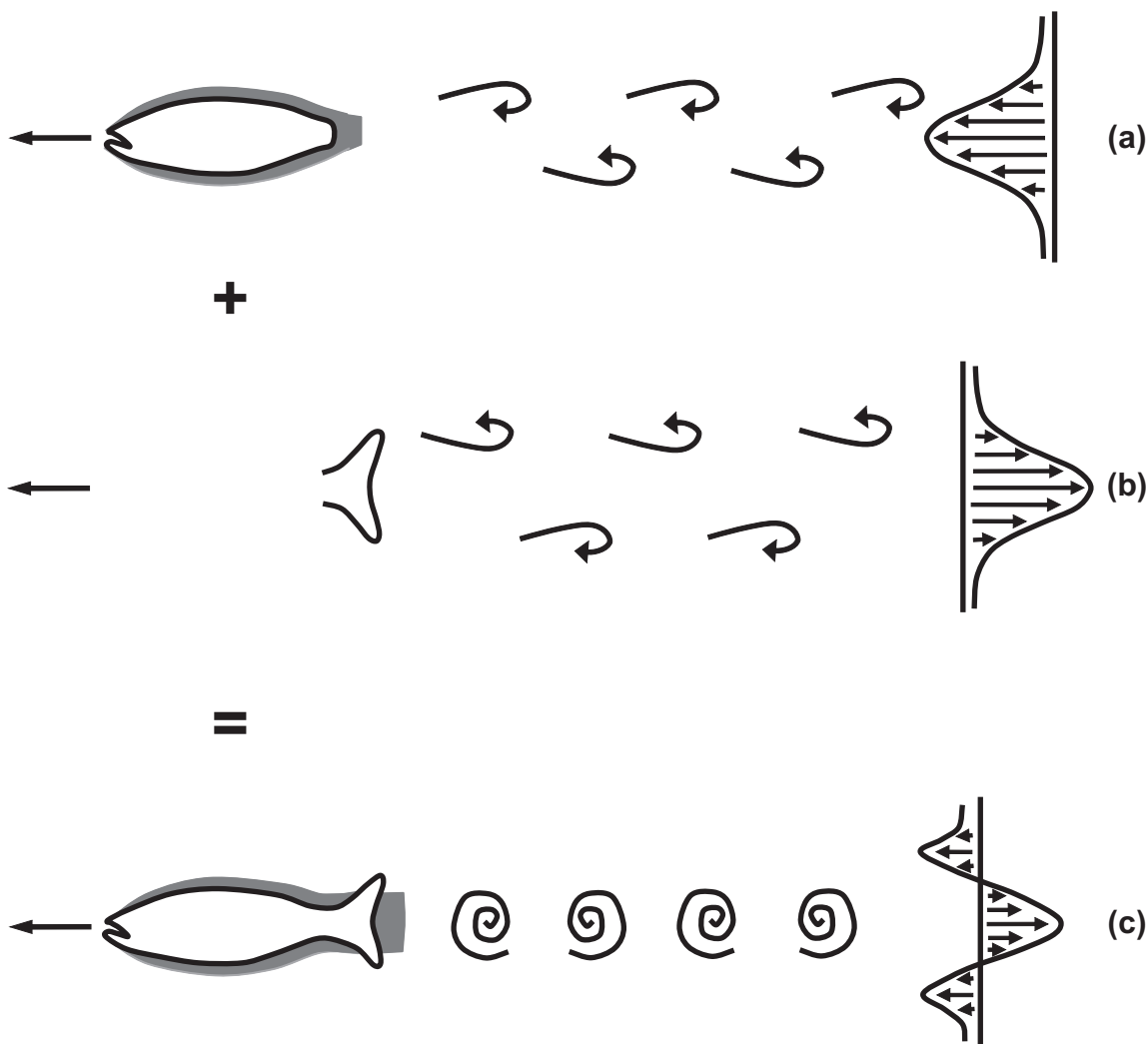
Here u is the velocity of the fluid generated in the stationary fluid when the body moves through it with velocity U_b ; u is taken as positive when it is in a direction opposite to the body motion direction. The area integral is taken over a plane, normal to the direction of motion of the body.

A drag producing body will drag the fluid along with it in the wake (F_x and u are negative)

(figure 13a), while a thrust producing body, for example, a propeller or flapping fin (figure 13b), moving in a stationary fluid will push the fluid in the backward direction (F_x and u are positive). In the case of a self propelling body moving at constant velocity, such as a steadily swimming fish, the net force is zero, and hence it leaves behind a momentum-less wake (figure 13c)! In this self-propelling case:

$$\iint_A \rho(u+U_b)u dA = 0 \quad (12)$$

Figure 13: The wake downstream of (a) the drag producing fish body, (b) thrust producing flapping tail (or propeller) and (c) the sum of the drag producing body and the thrust producing tail. In the case of a fish in steady forward motion (as in (c)), the net momentum in the wake is zero, as the drag on the body is balanced by the thrust from the tail. In all cases, the body is moving to the left through stationary fluid. The viscous boundary layer on the fish body is shown by the shaded dark region.



Energy considerations give an alternate and equally useful perspective. Taking the example of a propeller, the work done by the motor rotating the propeller (Torque * angular speed) goes into useful work (Thrust * U_b), into generation of kinetic energy of the fluid which flows into the wake and into **viscous dissipation**. (The kinetic energy of the fluid in the wake also gets converted into heat, but very far downstream for high Re flows.) A self propelling body, such as a fish moving with constant velocity, leaves behind a momentum-less wake, but which will have kinetic energy, and plenty of it, if it is an inefficient swimmer! For example, in figure 13c, work done (P_w) by the fish will go into viscous dissipation in the boundary layers on the body surface and into the kinetic energy left behind in the wake from fluid velocity components (u, v, w) in all three directions.

$$P_w = \iint_A \frac{\rho}{2} (u^2 + v^2 + w^2) (u + U_b) dA + \text{rate of viscous dissipation} \quad (13)$$

7. Wake Structure

In many cases, wakes of bodies moving in a fluid at high Reynolds numbers are best characterized by vortices (see box item 2). The Karman vortex street behind 2-D bluff bodies (Govardhan & Ramesh, 2005), the trailing vortices from wing-tips of aircraft (often seen as two white trails in the sky) and the helical vortices from the tips of propeller blades (fig. 14) are common examples.

Vortices carry both momentum and kinetic energy, and are often used in modeling such flows; for example, drag force on a circular cylinder in cross flow may be estimated, as first done by Kármán (see Kármán, 1954), from the circulation values around each vortex and the spacing characteristics between vortices. Vortices are generally formed from boundary layers separating from the surface of a body and from boundary layers coming off sharp edges such as those of wings and propeller blades.

In the case of wakes of fish, it is important to recognize the two main phenomena, arising out of Kelvin's and Helmholtz laws, that produce the vortices observed in the wake. The first phenomenon is connected to the fact that a periodic flapping of an airfoil produces a periodically varying lift force, and correspondingly a periodically varying circulation around the tail cross-section (see equation 9). Compensatory circulation is shed in the wake, which is seen usually as a pair of counter-rotating vortices for every cycle of flapping. Figure 15 shows such vortices behind an oscillating airfoil. The second phenomenon is related to shedding of vortices at the wing tips, such as the trailing vortices from an aircraft or the helical vortex from a propeller blade tip (fig. 14). Flapping fish tails show a combination of these two effects to produce a series of vortex rings which are left behind in the wake. The geometrical arrangement of the vortex rings reveals the nature of the wake. The flapping lunate tail (figure 16) produces interconnected alternate signed vortex rings producing an undulating backward jet; the momentum in the jet is directly related to the thrust from the tail which overcomes the drag force on the rest of the fish's body. Vorticity is also shed from the drag producing part of the body, which eventually interacts with the vortex rings, to produce a momentum-less wake. The wake structure in anguilliform swimming is much more complicated. Measurements (Tytell & Lauder, 2004) show rings with their axes perpendicular to the direction of motion; these rings produce lateral jets, and thus no thrust or drag (figure 17). Computations reveal an even more complicated structure with strong interaction between body boundary-layer vorticity and the vortex rings produced by the tail (fig. 18). Lateral motion of the body also produces streamwise vorticity (figure 17b) along the body, leading to added inefficiencies. Pulsatile jet propulsion of squids, salps and others produces rings with axes aligned in the direction of motion and producing backward flow (thrust). In this case as well, vorticity from the

Viscous dissipation: Any fluid motion leads to production of heat or thermal energy due to viscous dissipation; within a fluid volume, the rate of energy dissipation being ultimately related to the square of the velocity gradients in the flow (Batchelor, 1967). For example, a liquid stirred in a container eventually loses all its kinetic energy into heat and becomes still by this mechanism. Note that viscous dissipation is large in regions with large velocity gradients, such as boundary layers; turbulent flows with large internal velocity gradients are notoriously dissipative.

Figure 14: The wake of a propeller consists of a pair of helical vortices one emanating from each tip of the propeller. These helical vortices are in principle similar to the wing tip vortices seen behind a wing on an aircraft.

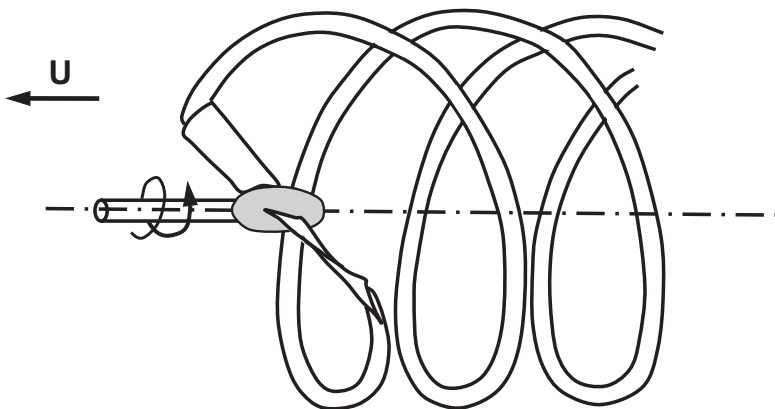
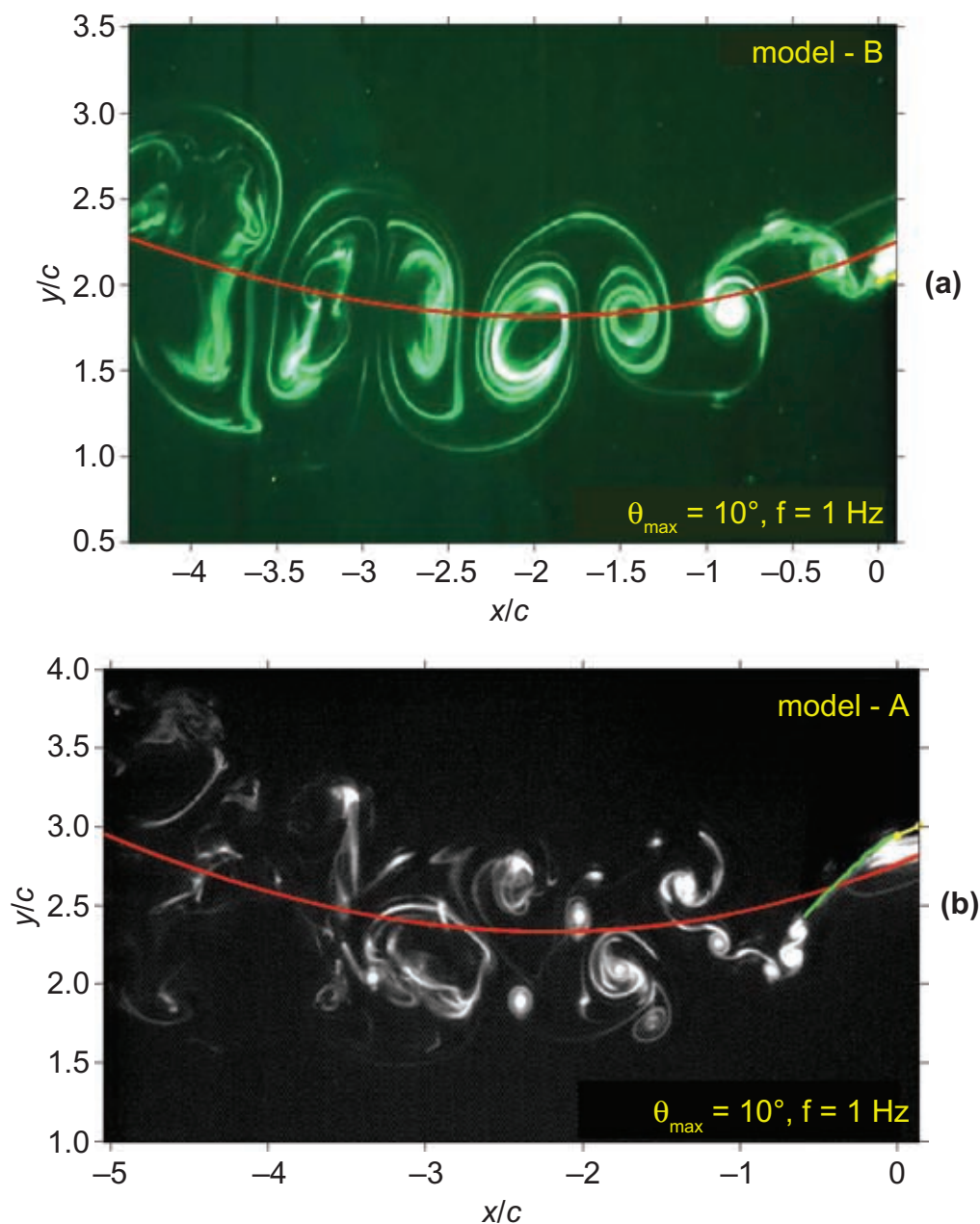


Figure 15: Dye visualization of the wake of an oscillating (a) rigid and (b) rigid foil with flexible flap (Shinde, 2007). In both cases, the foil oscillations are in pitch (angular) about mean value of zero, while moving in a wide circular arc. In (a), the oscillations are close to the self-propelling condition (drag = thrust) and hence the vortices are aligned along the mean line of motion of the foil. In (b), there are many small vortices produced by the flexible flap at the aft of the rigid foil.



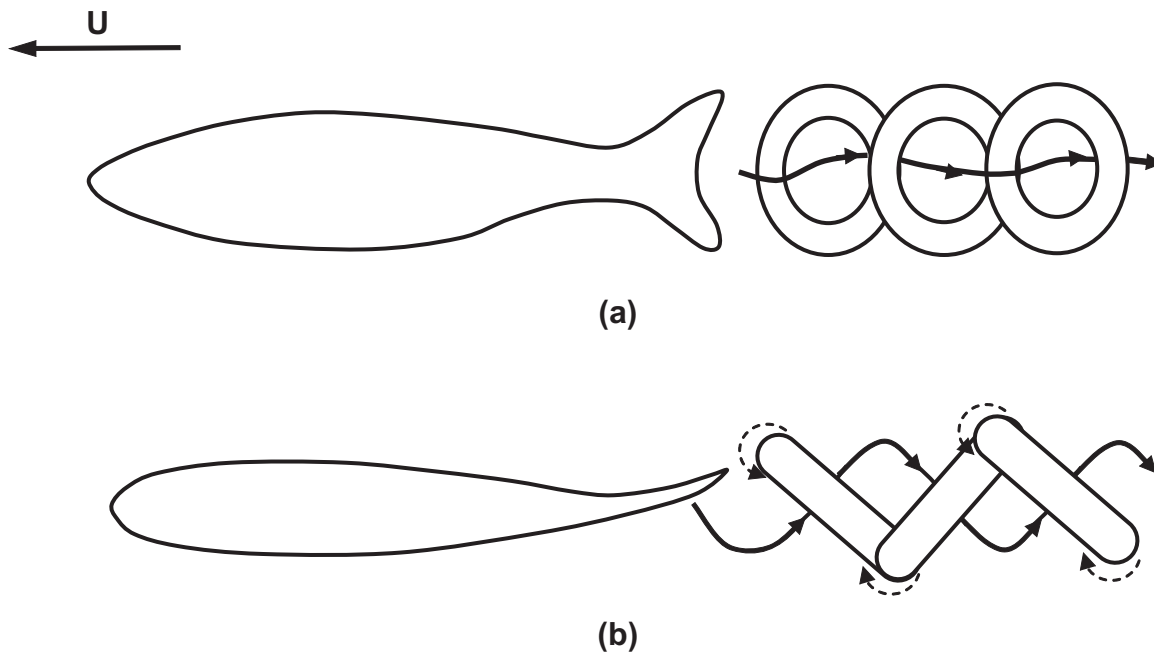
boundary layers and the rings will interact to give a momentum-less wake.

8. Discussion and Conclusion

We have presented three common types of thrust generation in aquatic animals swimming at high Reynolds numbers. In the anguilliform or eel type

swimming, an undulatory wave runs down the body from head to tail (figure 5) with the wave speed greater than the forward swimming speed of the animal. Linearized inviscid flow theories (Lighthill, 1960; Wu, 1961) and Lighthill's reactive flow theory (Lighthill, 1975) predict that the thrust is essentially a reaction force on the tail

Figure 16: The wake of a flapping fish tail consists of interconnected alternating signed vortex rings. (a) Side view and (b) top view. The sense of rotation of the vortex rings in the central plane is shown by the dashed arrows. These vortex rings generate an undulating backward jet.



due to acceleration of water as it passes by the tail; on the rest of the undulating body, forces cancel out over one cycle and no net thrust or side force are produced. In thunniform swimming with the crescent shaped lunate tail, characteristic of fast swimmers like some sharks, the thrust is mainly from the lift force on the airfoil like tail cross-section; the tail constantly changes orientation as it flaps back and forth so that the right angle of attack is maintained. In the third type of swimming mode, pulsed or transient jets produce thrust due to two reasons, one from the commonly known ejection of momentum from the exit as in a rocket, and second, peculiar to transient jets, due to an over pressure at the exit when the flow accelerates in first half of each pulse. Both reactive force generation and overpressure are from the so-called added mass effect, which can be thought of as an inertial force required to accelerate the fluid surrounding an accelerating object (Box item 2).

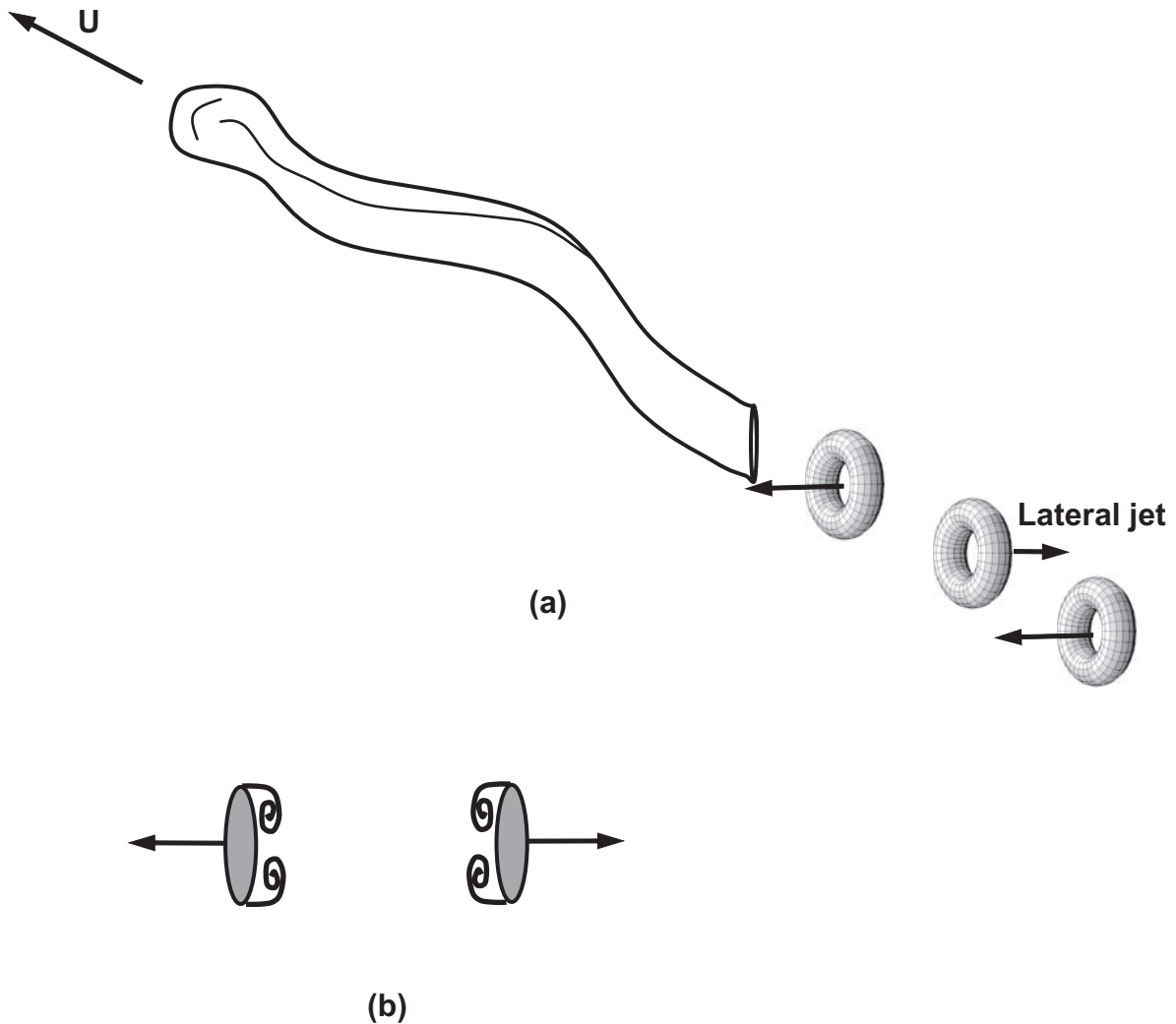
An important question that is often asked, is what is the efficiency of a self-propelled body, and how do natural ones compare with man-made ones. In the aircraft, for example, and in some aquatic animals like the lunate-tail and jet propelled swimmers, thrust producing and drag producing elements are quite distinct. In these

cases, best performance would be expected with a low drag (streamlined) body, like that of a shark, and the most efficient propulsor. On a streamlined body, flow does not separate, boundary layers are attached, and drag (D) is mainly due to viscous tangential stress, $D = 1/2 C_d \rho U_b^2 A_s$, $C_d \sim 0.01$.

For 'pure' propulsors, like a propeller or the lunate fish tail, a propulsive efficiency may be defined as the useful work done by the propeller (TU_b) divided by the work done on the propulsor. As discussed earlier, rest of the work done on the propulsor goes into viscous dissipation and kinetic energy (equation 13). Thrust (T) may generally be written as a product of the fluid mass flow rate and change in velocity, $T = \dot{m} \Delta u$. Thrust may be increased by increasing mass flow rate (\dot{m}) or by increasing Δu . A larger Δu means more wasted kinetic energy into the wake; a larger mass flow rate would require a larger frontal area. Thus, larger diameter propellers or wider lunate tails would have a higher efficiency. A propulsor which produces a large Δu will be less efficient but more compact. A salp throwing out a large amount of water with low velocity is more efficient than a squid ejecting a high speed jet through a small exit.

But there are some issues even in aquatic animals with nearly distinct drag and thrust producing parts. Getting estimates of or measuring

Figure 17: Schematic of the wake vortex dynamics downstream of a swimming eel. (a) The dominant vorticity downstream of the eel are a series of vortex rings aligned with the direction of motion of the eel. The induced velocities due to these vortex rings form lateral jets that point in alternating lateral directions due to their alternating sense of rotation. (b) Cross-section of the eel body showing the alternating lateral motion (perpendicular to the motion direction) of a fixed part of the eel body. This motion, generates vorticity whose axis is along the flow direction (streamwise vorticity), which is also superposed on the vortex rings shown in (a).

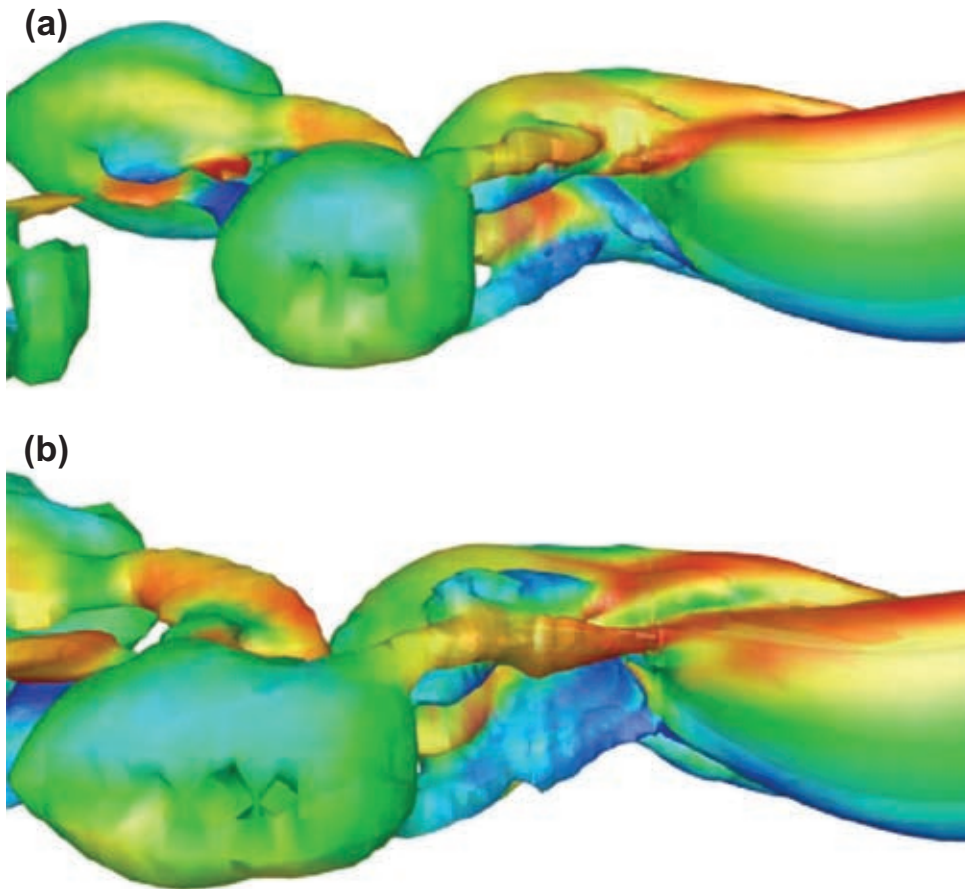


drag force on a fish body is problematic. The common method of measuring drag force on a towed dead fish is likely to give a very different value from the one on a live swimming fish. The boundary layers, which mainly dictate the viscous stress at the surface and the drag force, are likely to be very different on a live undulating fish body than on a rigid dead one. Simulations of boundary layers on wavy surfaces undergoing lateral oscillations in the form of a travelling wave show that the turbulence levels can be reduced significantly when the wave speed is large compared to the fluid velocity (Shen et al., 2003). Experiments in a water tunnel with a robotic fish

(Barrett et al., 1999), having wavy motions similar to a fish, showed power requirement, under certain conditions, to be lowered by about 40% when compared to the power required to tow a rigid body. Several robotic fishes have been built (Triantafyllou & Triantafyllou, 1995; Barrett et al., 1999) replicating as completely as possible the swimming kinematics of real fish.

A second issue is related to the caudal fins and may be a significant factor in thrust generation. Is a flexible fin better than a rigid one? There have also been some recent experiments (Heathcote & Gursul, 2007; Shinde, 2007) that show that simple flexibility, say in an oscillating airfoil of the type

Figure 18: Flow structure near the tail of a swimming eel from fluid flow simulations of Kern & Koumoutsakos (2006). Reproduced with permission from the Company of Biologists (S. Kern and P.Koumoutsakos, (2006), "Simulations of optimized anguilliform swimming", *J. Exp. Biol.* 209, 4841-4857.) The figure shows iso-surfaces of vorticity for (a) efficiently swimming eel and (b) for fast swimming eel.



seen in the thunniform mode of swimming, can be beneficial for thrust production.

In anguilliform swimmers, the demarcation between thrust and drag producing elements is even less certain. Numerical simulations (Kern & Koumoutsakos, 2006) show that elements in the central length of the body experience both thrust (forward force) and drag (backward force) at different times in the cycle in contrast to predictions of ideal flow theory. Indeed one may think of a system where each element of the body moves in such way that there is local balance of forces. In fact, at the most fundamental level, a question can be asked which is the best geometrical shape and motion of that shape that produces the 'best' (constant velocity) swimmer. From an energy point of view, the body and its motion should be such that it produces least viscous dissipation, and apart from the momentum-less wake, it should

leave behind a minimum energy wake, ideally a zero energy one.

This brings us back to the issue of efficiency in self propelling bodies, when taken as a whole. When a self propelling body moves in a horizontal plane, no work is done as the net force on the body is zero; no potential or kinetic energy is gained. Thus the conventional definition will always give an efficiency equal to zero! (A horse pulling a cart does useful work in overcoming the friction on the wheels of the cart. However the horse-cart system does no useful work.) To compare different locomotion systems, a non-dimensional measure has been suggested, Cost of Transport (COT) (see Vogel, 1988; Videler, 1993), defined as,

$$\text{COT} = \frac{P_i}{W U_b} \quad (14)$$

Table 2: Cost of transportation (COT) (Vogel, 1988; Videler, 1993) values for various aquatic organisms. The COT values given are non-dimensional and represent the energy expended by the organism to move a certain distance horizontally compared to the work done in moving the same distance vertically against gravity. The table is organized in decreasing values of COT, and also includes the mass and the optimal speed of the organism. The largest COTs are for squids, while the smallest values are for the very large whales and perhaps surprisingly the small salps. Data source: ¹Videler, 1993 (compilation); ²Madin (1990).

Species	Mass (kg)	u_{opt} (m/s)	COT (J/Nm)
Squid (<i>Loligo opalescens</i>) ¹	0.041	0.37	1.26
Largescale mullet ¹	0.0083	0.21	0.67
Green turtle (<i>Chelonia mydas</i>) ¹	1.15	0.49	0.31
Rainbow trout (<i>Oncorhynchus mykiss</i>) ¹	0.264	0.28	0.29
Lake whitefish (<i>Coregonus clupeaformis</i>) ¹	0.364	0.46	0.18
Spotted seatrout (<i>Cynoscion nebulosus</i>) ¹	0.35	0.81	0.18
Bonnethead shark (<i>Sphyrna tiburo</i>) ¹	4.65	0.48	0.17
Salp (<i>Cyclosalpa polae</i> solitary) ²		0.03	0.16
Bottlenose Dolphin (<i>Tursiops truncatus</i>) ¹	145	4	0.14
Salp (<i>Salpa fusiformis</i> solitary) ²		0.07	0.06
Gray Whale (<i>Eschrichtius robustus</i>) ¹	15000	2.25	0.04

where P_i is the rate of energy consumption by a moving animal, W is its weight in Newtons and U_b its velocity. (Defined this way COT is non-dimensional; sometimes, W is in kg, in which case COT is not non-dimensional.) COT may be thought of as the ratio of energy spent in moving a certain (horizontal) distance to the potential energy gained, or the work done against gravity, if the same body moved the same distance vertically upward. There is no rational reason for this definition, especially in the case of swimming where gravity does not play a role, but it allows for interesting comparisons. Note that speed of locomotion does not enter in the definition of COT. For all three classes of locomotion, terrestrial, aerial and aquatic, COT goes down inversely with mass. Trains and Ocean liners have the least COT (about 0.01); a jumbo jet has 0.2; a runner (COT = 0.12) spends three times more energy than a cyclist (COT = 0.04). For aquatic organisms, table 2 lists COT values for several aquatic species. It may be seen that a number of fishes have COTs in the range of 0.2 to 0.3, with the lowest value being for the very large whale (~0.02). Further, the COT value for some salps is also very low (0.06) and is very high for squids (1.26), perhaps for the reasons discussed earlier with reference to pulsed jet propulsion.

Finally, it is important to remember that fish (and other live natural systems) have evolved to survive and reproduce in the highly varied environments that they encounter. Thus the fins and tails will not be optimal just, for example, for efficient swimming. Fast starts and stops, intricate maneuvering could be equally important. Similarly, low drag, though important, may not be

the top priority for the skin of shark; it has many other functions. Our current understanding of fish swimming hydrodynamics is unable to answer the question whether lunate tail propulsion is better than a propeller based one. Due to the many unanswered questions, and the possible benefits that such understanding could bring to man-made underwater vehicles, fish swimming and more generally aquatic locomotion continue to be an active area of research.

Received 10 October 2011.

References

- Nelson, J.S. *Fishes of the world* (John Wiley & Sons, Inc., Hoboken, New Jersey, 2006).
- Subramanian, G., Nott, P., 2011 (Article from same issue of IISc Journal).
- Triantafyllou, M.S., Triantafyllou, G.S., Yue, D.K.P., *Annu. Rev. Fluid Mech.*, 2000, 32, 33.
- Fish, F.E., Lauder, G.V., *Annu. Rev. Fluid Mech.*, 2006, 38, 193.
- Wu, T.Y. *Annu. Rev. Fluid Mech.*, 2011, 43, 25.
- Lighthill, M.J., 1975. *Mathematical Biofluidynamics*. Philadelphia: SIAM
- Videler, J.J., 1993 *Fish swimming*. London: Chapman & Hall.
- Lindsey, C.C. *Fish Physiology*, Volume VII, Locomotion (Academic Press, New York, 1978) 1, 88.
- Marey, E.J., "Movement." Heinemann, London, 1895.
- Breder, C.M., Jr. (1926). *The locomotion of fishes*. *Zoologica* (N.Y.) 4, 159, 256.
- Gray, J. J. *Exp. Biol.*, 1933, 10, 88.
- Lauder, G.V., Tytell, E.D. *Fish Biomechanics*. Volume 23 in *Fish Physiology*, 425–468, 2006.
- Triantafyllou, G.S., Triantafyllou, M.S., Grosenbaugh, M.A. *J. Fluids Struct.*, 1993, 7, 205.
- Triantafyllou, M.S., Triantafyllou, G.S. *Sci. Am.*, 1995, 272, 64.
- Gray, J. J. *Exp. Biol.*, 1936, 13, 192.

16. Batchelor, G.K.; An Introduction to fluid Mechanics (Cambridge University Press, 1967).
17. Tytell, E.D., Lauder, G.V. *J. Exp. Biol.*, 2004, 207, 1825.
18. Tytell, E.D. *J. Exp. Biol.*, 2004, 207, 3265.
19. Kern, S., Koumoutsakos, P. *J. Exp. Biol.*, 2006, 209, 4841.
20. Lighthill, M.J. *J. Fluid Mech.*, 1960, 9, 305.
21. Wu, T.Y. *J. Fluid. Mech.*, 1961, 10, 321.
22. Wu, T.Y. In *Biomechanics: Proc. Symp. Biomech.*, ed. YC Fung, 1966, 187.
23. Lighthill, M.J. *Proc. R. Soc. Lond. B.*, 1971, 179, 125.
24. Anderson, J.M., et al. *J. Fluid Mech.*, 1998, 360, 41.
25. Bartol, I.K., et al. *J. Exp. Biol.*, 2001, 204, 3655.
26. Madin, L.P. *Can. J. Zool.*, 1990, 68, 765.
27. Didden, N. *J. Appl. Math. & Phy.*, 1979, 30, 101.
28. Gharib, M., et al. *J. Fluid Mech.* 1998, 360, 121.
29. Linden, P.F., Turner, J.S. *J. Fluid Mech.*, 2001, 427, 61.
30. Norbury, J. *J. Fluid Mech.* 1973, 57, 417.
31. Krueger, P.S., Gharib, M. *Phy. Fluid*, 2003, 15, 1271.
32. Linden, P.F., Turner, J.S. *The Royal Society*, 2004, 271, 647.
33. Dabiri, J.O. *Annual Rev. Fluid Mech.*, 2009, 41, 17.
34. Sharadha, V., Arakeri, J.H., *Resonance*, 2004, 9, 66.
35. Glezer, A., Amitay, M., *Annu. Rev. Fluid Mech.*, 2002, 34, 503.
36. Colin, S.P., Costello, J.H. *J. Exp. Biol.*, 2002, 205, 427.
37. Dabiri, J.O., et al. *J. Exp. Biol.*, 2005, 208, 1257.
38. Anderson, E.J., Grosenbaugh, M.A. *J. Exp. Biol.*, 2005, 208, 1125.
39. Johnson, W., et al. *J. Exp. Biol.*, 1972, 56, 155.
40. Anderson, E.J., Demont, M.E. *J. Exp. Biol.*, 2000, 203, 2851.
41. Krueger, P.S., et al. *J. Fluid Mech.*, 2006, 556, 147.
42. Prandtl, L., Tietjens, O.G., *Fundamentals of Hydro and Aeromechanics*, Dover Publications, 1957.
43. Govardhan, R.N., Ramesh, O.N.; *A Stroll down Kármán Street, Resonance.*, 2005, Vol. 10, No. 8.
44. Kármán, T., *Aerodynamics: Selected topics in the light of their historical development*. Cornell University Press, 1954.
45. Shen, L., et al., *J. Fluid Mech.*, 2003, 484, 197.
46. Barrett, D.S., et al., *J. Fluid Mech.*, 1999, 392, 183.
47. Heathcote, S. Gursul, I. *AIAA JOURNAL*, 2007, 45(5), 1066.
48. Shinde, S.Y., M.Sc thesis, Dept. of Mech. Engg., Indian Institute of Science (2007).
49. Vogel, S. *Life's Devices: The Physical World of Animals and Plants*, Princeton University Press, 1988.
50. Blevins, R.D. *Flow-Induced Vibrations*, Krieger Publishing Company, Florida, 2001.
51. Newman, J.N., *Marine hydrodynamics*. Cambridge, Massachusetts: MIT Press, 1977.
52. Lighthill, M.J. (1986). *An informal introduction to theoretical fluid mechanics*. Oxford: Clarendon Press.



Jaywant H. Arakeri has been in the faculty in the India Institute of Science since 1988. He is currently a professor in Mechanical Engineering and Centre for Product Design and Manufacture. His research interests are in Fluid Mechanics and Heat Transfer, in particular stability, transition and turbulence, unsteady flows, turbulent natural convection, solar energy and ventilation. He is also interested in writing popular science articles and in experiments for school children, and is an Associate Editor of *Resonance*, a journal of science education.



Raghuraman N. Govardhan has been at the Department of Mechanical Engineering at the Indian Institute of Science since 2003, where he is presently an Associate Professor. His research interests are in the areas of fluid-structure interaction, separated flows and micro-flows.